The phycobilisome protein ApcG interacts with photosystem II and regulates energy transfer in *Synechocystis sp.* PCC 6803

Roberto Espinoza-Corral[a,d]; Masakazu Iwai[c,e]; Tomáš, Zavřel[g]; Sigal Lechno-Yossef[a,d]; Markus Sutter[a,b,c]; Jan Červený[g]; Krishna K. Niyogi[c,e,f] and Cheryl A. Kerfeld[a,b,c,d]*.

[a]MSU-DOE Plant Research Laboratory, Michigan State University, East Lansing, MI, USA

[b]Environmental Genomics and Systems Biology Division, Lawrence Berkeley National Laboratory, Berkeley, CA, USA

[c]Molecular Biophysics and Integrated Bioimaging Division, Lawrence Berkeley National Laboratory, Berkeley, CA, USA

[d]Department of Biochemistry and Molecular Biology, Michigan State University, East Lansing, MI, USA

[e]Department of Plant and Microbial Biology, University of California, Berkeley, CA, USA

[f]Howard Hughes Medical Institute, University of California, Berkeley, CA, USA

[g]Department of Adaptive Biotechnologies, Global Change Research Institute of the Czech Academy of Sciences, Brno, Czech Republic

*To whom correspondence should be addressed:
Cheryl A. Kerfeld: ckerfeld@lbl.gov

Keywords: Phycobilisomes, Photosystem, *Synechocystis*, State transitions, light harvesting

Abbreviations: PS: photosystem; PBS: phycobilisomes; APC: allophycocyanin

ABSTRACT

Photosynthetic organisms harvest light using pigment-protein complexes. In cyanobacteria, these are water-soluble antennae known as phycobilisomes (PBSs). The light absorbed by PBS is transferred to the photosystems in the thylakoid membrane to drive photosynthesis. The energy transfer between these complexes implies that protein-protein interactions allow the association of PBS with the photosystems. However, the specific proteins involved in the interaction of PBS with the photosystems are not fully characterized. Here, we show that the newly discovered PBS linker protein ApcG interacts specifically with photosystem II through its N-terminal region. Growth of cyanobacteria is impaired in *apcG* deletion strains under light-limiting conditions. Furthermore, complementation of these strains using a phospho-mimicking version of ApcG exhibit reduced growth under normal growth conditions. Interestingly, the interaction of ApcG with photosystem II is affected when a phospho-mimicking version of ApcG is used, targeting the positively charged residues interacting with thylakoid membrane suggesting a regulatory role mediated by phosphorylation of ApcG. Low temperature fluorescence measurements showed decreased photosystem I fluorescence in *apcG* deletion and complementation strains. The photosystem I fluorescence was the lowest in the phospho-mimicking complementation strain while pull-down experiment showed no interaction of ApcG with PSI under any tested condition. Our results highlight the importance of ApcG for selectively directing energy harvested by the PBS and implies that the phosphorylation status of ApcG plays a role in regulating energy transfer from PSII to PSI.

62 **INTRODUCTION**

63 Light harvesting in cyanobacteria and red algae is enhanced by soluble protein-pigment
64 complexes known as phycobilisomes (PBSs). The energy absorbed by PBSs is
65 transferred to photosystem II (PSII) and photosystem I (PSI) embedded in the thylakoid
66 membrane. In the model cyanobacterium *Synechocystis sp.* PCC 6803 (hereafter
67 referred to as *Synechocystis*), the PBS consists of a tri-cylindrical core with six attached
68 rods, in a hemidiscoidal arrangement (Dominguez-Martin et al., 2022, Gantt and Conti,
69 1969, Bryant et al., 1979). The PBS consist of phycobiliproteins containing covalently
70 linked bilin pigments and assembled into disc-like trimers $(\alpha\beta)_3$ or hexamers $(\alpha\beta)_6$, and
71 colorless linker proteins that connect the phycobiliprotein discs (Adir, 2005, Glauser et
72 al., 1992, Anderson and Toole, 1998, de Marsac and Cohen-bazire, 1977). Their size and
73 the ability to absorb light at wavelengths between 550 to 650 nm, where chlorophyll *a*
74 absorption is low, increases the area and the spectral range of light harvesting in
75 cyanobacteria.

76 The energy transfer from water-soluble PBS to the photosystems entails a close contact
77 between these complexes. A recent structure of the PBS-PSII super-complex (with a
78 resolution of 14.3 Å) from the red algae *Porphyridium purpureum* UTEX 2757 provides
79 insights on the architecture of this interaction, involving allophycocyanin E (ApcE, also
80 classified as core-membrane linker protein L_{CM}), allophycocyanin D (ApcD) and three
81 unidentified connector proteins from PBS (Li et al., 2021). These phycobiliproteins have
82 been classified as terminal emitters responsible for energy transfer to PSII (ApcE) and
83 PSI (ApcD) (Gindt et al., 1992, Dong et al., 2009, Peng et al., 2014, Liu et al., 2013).
84 Additionally, pull-down experiments followed by mass-spectrometry of PBS and
85 photosystems from *Synechocystis* have shown putative contact sites in the interface of
86 these super-complexes involving also ApcD and ApcE (Liu et al., 2013).

87 Furthermore, PBSs and photosystems have been observed to be organized into three
88 main microdomains in the thylakoid membrane, one containing the trimeric PSI, another
89 one with the dimeric PSII and PBS, and the last one including both photosystems and
90 PBS (Straskova et al., 2019). Additionally, cryogenic electron tomography of
91 *Synechocystis* has shown that PBSs organize in arrays on the thylakoid membrane,
92 presumably increasing the efficiency of light harvesting (Rast et al., 2019). While PBSs

are able to transfer energy to either PSII or PSI, the proteins involved in PBS-PSII or PBS-PSI interactions that govern such specificity are still unknown. Moreover, energy transfer from PBS to PSI could follow two plausible models. On the one hand there is the model of PBS mobility on thylakoid membranes that assumes detachment of PBS from PSII to then attach to PSI (Sarcina et al., 2001, Mullineaux et al., 1997, Yang et al., 2007). On the other hand, the spillover model proposes that the energy absorbed by PBS is first transferred to PSII, which then transfers the excess of energy to PSI (McConnell et al., 2002, Folea et al., 2008, Olive et al., 1997). There is an efficient mechanism for short timescales regulation of photosystems activity in response to variations in both the quality and quantity of light known as state transitions. This process aims to prevent photodamage caused by the saturation of the photosynthetic electron transport chain, ensuring a balanced activity of both PSI and PSII. In contrast to plants, there is little consensus on how state transitions are achieved and regulated in cyanobacteria (Calzadilla and Kirilovsky, 2020).

The *Synechocystis* PBS structure recently obtained by cryogenic electron microscopy (Cryo-EM, with a resolution of 2.1-3.5 Å) included different rod conformations and revealed a novel PBS linker protein (ApcG) located at the bottom two cylinders of the tri-cylindrical core (Dominguez-Martin et al., 2022). Due to its location in the PBS core, it has been hypothesized that this linker protein could interact with the photosystems allowing the tethering of PBS to the thylakoid membrane.

Here we show that the PBS linker protein ApcG binds specifically to PSII via its N-terminal region and that this interaction is likely affected by the phosphorylation state of ApcG. Furthermore, an *apcG* deletion strain shows slower growth compared to wild type under light-limiting conditions. Under normal light conditions only a phospho-mimicking *apcG* complementation strain shows slower growth. This phenotype was further characterized by low temperature fluorescence, revealing an imbalance in PSII and PSI activity in the deletion and complementation strains, which exhibited lower PSI fluorescence with the lowest in the phospho-mimicking version of ApcG. Our results indicate that ApcG plays a crucial role in PBS-PSII interaction and the transfer of energy towards PSI, presumably via the “spillover” mechanism.

124 **RESULTS**

125 **Domain organization of ApcG**

126 The recent *Synechocystis* PBS structure showed that two ApcG molecules bind to the
127 PBS at the membrane-facing side, one at each of the bottom core cylinders via the C-
128 terminal domain of ApcG (**Figure 1A, B**) (Dominguez-Martin et al., 2022). The PBS-
129 binding domain is characterized by a conserved FxxM motif, which interdigitates with
130 ApcA at the bottom core cylinder (Liu, 2023) (**Figure 1A, C**). The location observed in the
131 Cryo-EM structure indicates that the N-terminal portion of ApcG extends outwards from
132 the PBS core, presumably to interact with the photosystems in the thylakoid membrane.
133 A sequence search indicated that ApcG homologues are found in 94% of cyanobacterial
134 genomes that also have an ApcE orthologue (Dominguez-Martin et al., 2022).
135 Additionally, proteomics data indicate that ApcG and ApcE expression levels are
136 comparable, with similar behavior under different light intensities (Zavrel et al., 2019).
137 The amino acid conservation of ApcG orthologs from various cyanobacteria species show
138 three conserved domains; i) N-terminal domain, ii) a positively charged middle domain
139 and iii) the PBS binding domain **(Figure 1C**). Additionally, phospho-proteomic data show
140 that ApcG contains several phosphorylation sites detected under low and high carbon
141 growth conditions (Angeleri et al., 2016). They are located close to the positively charged
142 middle domain, which could play a role in regulating this region's interaction with the
143 thylakoid membrane (**Figure 1B, D**). Specifically, residues 46-48 (TTS) were found to be
144 phosphorylated under low and high carbon conditions (Angeleri et al., 2016).
145 Furthermore, AlphaFold2 (Jumper et al., 2021) structure prediction of ApcG shows that
146 the middle domain is unstructured compared to the PBS-binding domain (**Figure 1D**).
147 The conservation of ~20 residues at the N-terminus (**Figure 1C**) suggests that it could
148 play a role in regulating the interaction of PBS with one of the photosystems.

149

150 **The phosphorylation status of ApcG impacts growth and activity of photosystems**
151 **in *Synechocystis***

152 In order to understand the physiological role of ApcG (*sll1873* gene locus), we generated
153 a deletion strain replacing the native coding sequence of *apcG* by a chloramphenicol
154 resistance cassette (Δ*apcG)*. Additionally, we complemented this deletion strain by

155 replacing the native *psbA2* gene copy (Englund et al., 2016) with the *apcG* wild type open
156 reading frame, and two phospho-mimicking versions to test the impact of the
157 phosphorylation sites in the positively charged domain (**Supp. Figure S1**). This strategy
158 ensures strong expression of the genes under the promoter of *psbA2* (P*psba2*) in
159 *Synechocystis*. Furthermore, the expression of *psBA2* under high light and under different
160 light qualities is similar to that of *apcG* and *psbA3* expression, enabling the comparison
161 of the complementation strains with wild type and mutant strains (Luimstra et al., 2020,
162 Cho et al., 2021). The generation of ApcG versions for testing the impact of its
163 phosphorylation sites was achieved by mutating codons coding the residues 46-48 from
164 *apcG* to glutamic acid (phospho-mimicking, TTS/EEE) or to alanine (permanent non-
165 phosphorylated, TTS/AAA). Growth of wild type and *apcG* deletion strains showed no
166 differences under normal conditions (constant light, 30 µmol photons $m^{-2}\cdot s^{-1}$) as well as
167 under stress conditions such as high light (400 µmol photons $m^{-2}\cdot s^{-1}$ light intensity) and
168 light to dark intervals (12 h light and 12 h darkness; **Supp. Figure S2**). However, when
169 the deletion strain was grown under light-limiting conditions (10 µmol photons $m^{-2}\cdot s^{-1}$),
170 its growth was strongly impaired compared to the wild type (**Figure 2A**). Furthermore,
171 when complemented with the phospho-mimicking $apcG^{TTS/EEE}$ growth was delayed during
172 exponential phase under both 10 and 25 µmol photons $m^{-2}\cdot s^{-1}$ compared to the deletion
173 mutant and the other complementation strains (**Figure 2A**). Additionally, comparison of
174 the strain's growth using blue light (450 nm), green light (530 nm), red light (615 nm,
175 exciting PBS) and far-red light (730 nm, exciting PSI) (Fuente et al., 2021) showed that
176 the phospho-mimicking $apcG^{TTS/EEE}$ strain only shows reduction in growth when using red
177 and far-red light, which could indicate an imbalance in the activity of the photosystems
178 (**Supp. Figure S3**). Whole-cell absorption spectra of wild type and *apcG* deletion and
179 complementation strains cultivated under normal conditions (i.e., white light of intensity
180 25-30 µmol photons $m^{-2}\cdot s^{-1}$) were similar (**Figure 2B, 2C**). Analyses of the pigments
181 present in the strains revealed that the phospho-mimicking strain contains a higher ratio
182 of carotenoids to chlorophyll, reduced overall chlorophyll and carotenoid content, however
183 no difference in phycobiliprotein content compared to wild type (**Figure 2D**). Interestingly,
184 the ratio of carotenoids and chlorophyll to culture turbidity, representing the amount of

185 pigments per cell, was lower in the phospho-mimicking strain compared to wild type and
186 the *apcG* deletion strain.
187 To gain further insight into the photosynthetic performance of the strains, low temperature
188 (77 K) fluorescence spectra were recorded. In these experiments, we added an additional
189 complementation strain using a construct coding for an *apcG* lacking the first 20 residues
190 (of the N-terminal domain, **Figure 1B**). Excitation of chlorophyll at 430 nm revealed a
191 decrease of PSI fluorescence at 728 nm in the *apcG* mutant compared to the wild type.
192 An even lower PSI fluorescence was observed in the complementation strains using the
193 phospho-mimicking $apcG^{TTS/EEE}$ accompanied with an increase in PSII fluorescence
194 compared to wild type and non-phosphorylated strains (**Figure 3A**). Interestingly, when
195 PBSs were excited at 590 nm, all strains showed reduced PSI and PSII fluorescence
196 (**Figure 3B**).
197 Since the *apcG* deletion, as well as phospho-mimicking $apcG^{TTS/EEE}$ showed striking
198 decrease in PSI fluorescence at 77 K, we investigated the possible role of ApcG in state
199 transitions. State I was induced in all tested *Synechosystis* strains by pre-treating the
200 cultures with blue light, and state II was induced by pre-incubating the cultures in
201 darkness. To monitor the differences in each state, 77 K fluorescence spectra of the
202 cultures were recorded by exciting PBS at 590 nm. Surprisingly, all strains showed the
203 same behavior as wild type under state I or II (**Supp. Figure S4**), indicating that the
204 imbalance of PSI and PSII observed by exciting chlorophyll *a* (**Figure 3A**) is not related
205 to state transitions.
206 Because the phospho-mimicking complementation strain showed lower PSI
207 fluorescence, we analyzed the steady-state levels of proteins from PBS, PSII and PSI.
208 Interestingly, immunoblots revealed no differences between strains in the levels of marker
209 proteins for PSI (PsaB), PSII (PsbA) and PBS (APC) (**Figure 4A**). In order to discard the
210 possibility that changes in the composition of thylakoid super-complexes could account
211 for the lower PSI fluorescence observed in the *apcG* deletion strain, we compared the
212 thylakoid super-complexes by blue native gels, which showed no differences between
213 wild type and the *apcG* deletion strain (**Figure 4B**). Additionally, isolated PBS from wild
214 type, *apcG* deletion and its complementation strains showed that the absence of ApcG
215 did not impact the absorbance or fluorescence spectra of PBSs (**Supp. Figure S5**).

216 Overall, our physiological comparison of *Synechocystis* strains shows that PBSs impairs
217 energy transfer towards PSI when ApcG is phosphorylated, indicating a regulatory role
218 impacting photosynthesis without disturbing the native organization of thylakoid super-
219 complexes.
220
221 **The N-terminal domain of ApcG binds PSII**
222 The structure of *Synechocystis* PBS shows that the C-terminal domain of ApcG binds to
223 one of the two bottom core cylinders but the N-terminal and middle domains are not
224 resolved (Dominguez-Martin et al., 2022). To investigate interaction partners of the N-
225 terminal portion, we designed a version of ApcG where the PBS-binding domain is
226 replaced by a His-tag (**Figure 5A**). This allowed both the rapid purification of the
227 recombinant protein from *E. coli* as well as performing pull-down experiments using nickel
228 affinity resin. We incubated *in vitro* ApcG bound to nickel resin with solubilized thylakoid
229 membranes and noticed that the eluate after washing was green. This was not observed
230 in the negative control (no ApcG). Immunoblot analyses to detect marker proteins for PSI
231 and PSII showed that proteins from PSII were pulled down with the truncated ApcG
232 (**Figure 5B**). The eluate was then separated on clear native (CN) gels showing the
233 presence of one specific complex (**Figure 5C**). A second dimension of SDS-PAGE from
234 the CN gel suggests that the complex found could correspond to PSII when compared to
235 thylakoid (**Figure 5D**). Indeed, immunoblots analyses of the CN gels using antibodies
236 against PsbA showed that it corresponds to PSII (**Figure 5E**). Additionally, immunoblots
237 using antibodies against the His-tag showed the presence of ApcG co-migrating with the
238 PSII complex, confirming their interaction (**Figure 5E**).
239 Our results using complementation strains with the phospho-mimicking version of *apcG*
240 suggest that phosphorylation of the positively charged domain of ApcG could impact its
241 interaction with the thylakoid complexes or the membrane. In order to assess this
242 possibility, we generated two additional versions of the truncated ApcG by mutating the
243 same residues used for the complementation strains, i.e., a permanent non-
244 phosphorylated (TTS/AAA) and a phospho-mimicking version (TTS/EEE). Pull-down
245 experiments showed a decrease of PSII proteins pulled down by the phospho-mimicking
246 version while wild type and the non-phosphorylated version showed a similar amount of

247 proteins from PSII (PsbA) being pulled down (**Figure 6A**). Furthermore, when using three
248 times the amount of phospho-mimicking (TTS/EEE) truncated ApcG for the pull-down
249 experiment relative to wild type and the permanent non-phosphorylated (TTS/AAA),
250 similar amounts of PsbA were pulled down. This implies that the ability of ApcG to interact
251 with PSII in the phospho-mimicking version (TTS/EEE) is reduced compared to the wild
252 type ApcG. The PSI core protein PsaB was not detected in any of the pull-downs,
253 indicating that neither wild type ApcG nor any of the phospho-mimicking mutants interact
254 with PSI (**Figure 6B**). In order to corroborate that the proteins pulled down corresponded
255 to the complex of PSII, CN gels were run using the same amount of protein loaded in
256 each lane and blotted to a membrane to detect PSII complexes using antibodies against
257 PsbA. Indeed, all three ApcG versions were able to pull down PSII complexes (**Figure**
258 **6C**). These results indicate that the N-terminal region of ApcG specifically interacts with
259 PSII while the phosphorylation of ApcG in its positively charge middle domain impairs the
260 ApcG-PSII interaction. Additionally, the phosphorylation of ApcG does not alter its
261 specificity for PSII.
262
263 **DISCUSSION**
264 In cyanobacteria, the energy transfer from PBS to the photosystems is known to have
265 several modes of regulation. For example, in response to high light there is the PBS
266 quenching mechanism mediated by the orange carotenoid protein, which dissipates the
267 excess of energy absorbed by PBS (Dominguez-Martin et al., 2022, Leverenz et al., 2015,
268 Kerfeld et al., 2017) thus reducing the likelihood of saturating the electron transport chain
269 in the thylakoid membrane. Likewise, as a response to differences in light quality, the
270 PBS can undergo state transitions by shifting between state I (PSII saturation or reduced
271 plastoquinone pool) and state II (PSI saturation or oxidized plastoquinone pool) to
272 balance the activity of both photosystems and prevent the accumulation of reduced
273 intermediates in the electron transport chain (Emlyn-Jones et al., 1999, Xu et al., 2012,
274 Bonaventura and Myers, 1969, Hodges and Barber, 1983). Cyanobacterial state
275 transitions, unlike those of plants, is not well understood. Several models have been put
276 forward to explain the mechanism behind this regulatory process. For example, the
277 “attachment/detachment” model in which PBS are released from PSII (state I) and interact

278 with PSI (state II) (Sarcina et al., 2001, Mullineaux et al., 1997, Yang et al., 2007). Another
279 model is the “spillover” mechanism in which PBS maintain their interaction with PSII, but
280 excitation energy spills over from PSII to PSI (McConnell et al., 2002, Folea et al., 2008,
281 Olive et al., 1997).
282 Several of our observations are consistent with a spill over mechanism. Our studies using
283 deletion and complementation strains for different version of ApcG showed that this linker
284 protein is indeed necessary for the efficient transfer of energy to drive photosynthesis,
285 especially under light-limiting conditions (10 µmol photons m^{-2} s^{-1} light intensity).
286 Furthermore, under normal conditions (25 µmol photons m^{-2} s^{-1} light intensity), the
287 phospho-mimicking *apcG*$^{TTS/EEE}$ strain showed delayed growth compared to all others
288 including the deletion *apcG* strain (**Figure 2A**). Comparison of the deletion and
289 complementation strains under increasing light intensities showed that the deletion of
290 *apcG* increases the maximal measured growth rate (μ_{max}) as well as the light intensity
291 necessary to saturate growth (I_S) (Platt et al., 1980) (**Supp. Figure S6**). Analyses of
292 pigment content showed an increase in carotenoid per chlorophyll ratio in the phospho-
293 mimicking *apcG*$^{TTS/EEE}$ strain (**Figure 2C**). Similarly, deletion mutants for proteins
294 affecting photosynthetic function in *Synechocystis* showed that indeed a higher
295 carotenoid per chlorophyll ratio is symptomatic of light stress with increased anti-oxidant
296 compounds content such as myxoxanthophyll and zeaxanthin (Cunningham et al., 2010,
297 Havaux et al., 2003, Maeda et al., 2005, Schafer et al., 2005). Strikingly, low temperature
298 fluorescence spectra of these strains displayed an decrease in PSI fluorescence when
299 exciting chlorophyll with the lowest one observed in the phospho-mimicking *apcG*$^{TTS/EEE}$
300 strain along with an increase in PSII fluorescence. This phenomenon was observed in
301 both the raw and normalized spectra among strains (**Figure 3A**). In order to discard that
302 the PSI fluorescence from wild type strain is due the expression of IsiA (because this has
303 been observed in conjunction with formation of PSI-IsiA super-complexes) (Bibby et al.,
304 2001b, Nagao et al., 2023, Bibby et al., 2001a, Burnap et al., 1993), we compared the
305 oligomeric state of thylakoid super-complexes from strains grown under normal and iron
306 deficiency conditions. Indeed, just under iron deficiency PSI-IsiA complexes can be
307 observed as well as reduction of PSI trimer (Duhring et al., 2006) compared to normal
308 conditions (**Supp. Figure S7**). Considering that (i) in these strains PBSs impact the PSI

309 fluorescence even when PBSs are not absorbing energy (**Figure 3A**) and (ii) among
310 strains, there is no difference in PSI accumulation or super-complex distribution to
311 account for the differences in PSI fluorescence (**Figure 4A**), the mechanism that best
312 accounts for these observations is "spillover". Furthermore, when observing low
313 temperature fluorescence spectra exciting PBS at 590 nm, all strains showed a reduced
314 PSII and PSI fluorescence indicating a less efficient energy transfer from PBS to
315 photosystems (**Figure 3B**). Thus, as a consequence of the phosphorylation of ApcG, our
316 results support an indirect effect of the PBS linker protein ApcG on the transfer of energy
317 from PSII towards PSI most likely via "spillover". The spillover model has generally been
318 associated with state transitions (McConnell et al., 2002, Li et al., 2006, Li et al., 2004).
319 However, our results show that the putative spillover involving ApcG does not play a role
320 in state transitions because all the mutant strains used in this study are able to transition
321 between state I and II, comparable to wild type (**Supp. Figure S4**). Therefore, the spillover
322 phenomenon observed in the *apcG* deletion as well as in the phospho-mimicking
323 *apcG*$^{TTS/EEE}$ strains implies that this process is not related to state transitions.
324 Nonetheless, these two mechanisms (spillover and attachment/detachment) could very
325 well happen in parallel, as it has been suggested (Mullineaux et al., 1997, Mullineaux,
326 2014, McConnell et al., 2002, Li et al., 2004, Li et al., 2006). Thus, the phenotype
327 observed under light-limiting conditions in the deletion *apcG* strain highlights the
328 imbalance in PSI and PSII, leading to decrease in the linear electron transport.
329 The PBS linker protein ApcG offers an opportunity to investigate the interface between
330 PBS and the membrane-embedded photosystems because of its position at the base of
331 the two core cylinders (Dominguez-Martin et al., 2022). Due to its occurrence along with
332 ApcE, which by its domain architecture defines the cylindrical core structure of PBS, the
333 function of ApcG in PBS might be quite conserved among cyanobacteria. Hence, ApcG
334 is expected to facilitate the interaction of PBS with complexes in the thylakoid membrane.
335 Our pull-down experiments using a truncated form of ApcG lacking the PBS binding
336 domain shows that the N-terminal region of the ApcG interacts with PSII from solubilized
337 thylakoids, presumably via the conserved domains of the N-terminus or the positively
338 charged middle region. Furthermore, in the ApcG$^{TTS/EEE}$ phospho-mimicking mutant
339 protein, the interaction with PSII is impaired. Additionally, the phospho-mimicking

340 *apcG$^{TTS/EEE}$* strain showed delayed growth (**Figure 2A**) suggesting that phosphorylation
341 could as well cause repulsion of the middle domain from the negatively charged head
342 groups of thylakoid lipids. Our results support a regulatory role for phosphorylation of
343 ApcG by altering the charge of the positively charged middle domain, which influences its
344 interaction with PSII (**Figure 6A**). Indeed, phosphorylation of other PBS proteins has been
345 reported (Toyoshima et al., 2020), (including ApcA, ApcC, ApcF, CpcA, CpcB) with CpcB
346 phosphorylation having a direct impact on state transitions (Chen et al., 2015).
347 Interestingly, 77K spectra after excitation of the PBS at 590 nm showed lower PSII and
348 PSI maxima among strains (**Figure 3B**), implying that ApcG is involved in the interaction
349 between PBS and PSII. This is supported by a red alga PBS-PSII structure that found
350 three unknown connector proteins in PBS (Li et al., 2021). As observed in low temperature
351 fluorescence spectra, PSI receives less energy in the *apcG* deletion and phospho-
352 mimicking *apcG$^{TTS/EEE}$* strains, pull-down experiments showed no accumulation of PsaB
353 (a core protein of PSI) (**Figure 6B**). These results suggest that the phosphorylation of
354 ApcG in its middle domain impairs the energy transfer from PSII to PSI through spill-over,
355 this phenomenon occurs without a direct physical interaction between ApcG and PSI.
356 Therefore, the effect that ApcG exerts on the fluorescence of PSI might be the result of
357 PSII-PSI interaction allowing the energy from PSII to spill over to PSI. Indeed, there is
358 experimental evidence for super-complexes involving PBS-PSII-PSI as well as PSII-PSI
359 except for PBS-PSI (Liu et al., 2013, Beckova et al., 2017, You et al., 2023). A super-
360 complex of PBS-PSII-PSI would allow spillover to occur; we observe evidence for ApcG
361 interacting solely with PSII yet affecting the energy transfer from PSII to PSI. A recent
362 PBS-PSII-PSI super-complex structure has been reported in red algae *Porphyridium*
363 *purpureum*; an ApcG homolog ($L_{pp}2$) is found in the super-complex interacting with a PSII
364 dimer. In contrast, the PSII-PSI interaction does not involve $L_{pp}2$ (You et al., 2023),
365 consistent with our observations (**Figure 3A and 6B**).
366 Our experiments explored the influence of phosphorylation using only ApcG point
367 mutations. Under similar growth conditions other proteins of a PBS-PSII complex might
368 also be phosphorylated. Indeed, PSII undergoes phosphorylation in several subunits
369 (PsbA, PsbB and PsbC) as well as for PSI (PsaA, PsaB, PsaC, PsaD, PsaE, PsaF, PsaL)
370 (Toyoshima et al., 2020, Angeleri et al., 2016). Thus, our results cannot exclude that ApcG

371 interacts with PSI or a PSI-PSII super-complex under conditions in which ApcG, as well
372 as subunits of PSI and PSII, undergo phosphorylation.
373 Collectively, our results show that the linker protein ApcG is necessary for efficient light
374 harvesting under light limiting conditions. While the C-terminal PBS-binding domain binds
375 to each of the two core bottom cylinders (Dominguez-Martin et al., 2022), its N-terminal
376 region interacts specifically with PSII as shown in our *in-vitro* pull down assays.
377 Furthermore, when phosphorylated in its positively charged middle domain, the
378 interaction of ApcG with PSII is hindered, which is correlated with a slower growth rate
379 (**Figure 2A and 6A**). The phosphorylation of ApcG in complementation strains showed a
380 decrease of energy absorbed by PSI even under conditions where PBS do not absorb
381 light, suggesting a role for ApcG in the spillover from PSII to PSI.
382
383
384 **MATERIALS AND METHODS**
385
386 **Cyanobacteria growth conditions**
387 *Synechocystis* sp. PCC 6803 strains were grown in BG-11 medium (Rippka et al., 1979),
388 buffered to pH 8 with 10 mM HEPES, at 28–30°C under constant light (25–
389 30 µmol photons m^{-2} s^{-1}) and enriched with 3% CO_2, unless otherwise stated, in shaken
390 liquid cultures (160 rpm). For selection of mutants on plates, BG-11 containing 3 g L^{-1}
391 sodium thiosulfate was solidified with 1.2% Difco agar. Antibiotic concentrations used for
392 selection of *Synechocystis* mutants were chloramphenicol at 25 µg ml^{-1}, or
393 spectinomycin at 20 µg ml^{-1}.
394 Cyanobacteria growth under these conditions (hereafter referred to as normal conditions)
395 was compared by cultivating the strains in flasks in batch regime starting with OD_{750} 0.05.
396 To apply light stress, the multi-cultivators (MC 1000-OD, Photon System Instruments,
397 PSI, Czech Republic) were used for cultivations under constant high light
398 (400 µmol photons m^{-2} s^{-1}) or for 12 hours darkness followed by 12 hours illumination
399 (30 µmol photons m^{-2} s^{-1}) for a period of 10 days.
400 The strains were further cultivated in Multi-cultivators MC-1000-MIX (Photon System
401 Instruments) in turbidostat regime, in BG-11 cultivation medium as described in the

402 previous section at 30 °C and at 0.5% CO_2. The strains were cultivated under 10, 25 and
403 100 µmol photons m^{-2} s^{-1} of warm white as well as green, red and far-red light under 25
404 and 100 µmol photons m^{-2} s^{-1}. The illumination was provided by LEDs with the following
405 peaks and half-bandwidths: blue: 450 ± 25 nm, green: 537 ± 40 nm, red: 615 ± 25 nm
406 and far-red: 730 ± 15 nm (**Supp. Figure S8**). The density range of the turbidostat
407 cultivation was set to OD_{720} 0.5 – 0.51, (approximately 10^7 cells mL^{-1}). The cultures were
408 cultivated under each light condition for at least 22 h, to secure full metabolic acclimation
409 (Zavrel et al., 2019). After the acclimation period, specific growth rates were estimated
410 from the change of OD_{720}.
411
412 **Generation of *Synechocystis* deletion and complementation strains**
413 The generation of deletion strain for *apcG* was done by amplifying the 600 base pairs
414 upstream as well as downstream its gene locus (Sll1873) using primers oREC1 (5'-
415 CCCTCAAACCCCAAACGATT) and oREC2 (5'-CGGGGCGAATGGTTTCTAAC) and
416 cloning into pJET1.2. The *apcG* gene was then replaced by a SacI site through inverse-
417 PCR using primers oREC3 (5'-GAGCTCTTTAATGTGGTTCTCCTAATTG) and oREC4
418 (5'-AAACCTCATTGATTTACTGTTTTATAC). This construct was used to introduce an
419 insert from pRL1075 compatible for bacterial conjugation and containing chloramphenicol
420 resistance cassette (Black et al., 1993). The insert was introduced by digestion and
421 ligation using SacI, resulting in the construct pSL399 for transformation of wild type
422 *Synechocystis*. For complementation strains, the open reading frame from *apcG* was
423 amplified with oREC9 (5'-TCGTCATATGTTAAAAAAATTGTTTGGCGCT) and oREC10
424 (5'-GTGCTCGAGACCGGAGCGTTTAACCTTAACTTGGCGAG) and cloned into pET-
425 28a(+) using restriction digestion enzymes BamHI and XhoI, resulting into the construct
426 pREC4. A region containing *apcG* from pREC4 was amplified using oREC11 (5'-
427 CCAATCCGGAGGATCCTATAGTTCCTCCTTTCAGCAA) and CK10 (5'-
428 TAATACGACTCACTATAGGG) and cloned into pPSBA2KS (Lagarde et al., 2000) using
429 restriction digestion enzymes BamHI and NdeI, resulting in the plasmid pREC6. A Bom
430 site compatible for bacterial conjugation was incorporated into pREC6 by inverse-PCR
431 and ligation using oREC25 (5'-
432 CACTCTCAGTACAATCTGCTCTGATGCCGCATCGAGCTCTGTACATGTCCGCGG)

433 and oREC26 (5'-
434 CACCATATGCGGTGTGAAATACCGCACAGATGAGAAGTACTAGTGGCCACGTGG)
435 resulting in plasmid pREC9. A spectinomycin resistance cassette was incorporated into
436 pREC9 by amplifying the *aadA* gene from pRL3332 (Nieves-Morion et al., 2017) using
437 oREC46 and oREC47 having BamHI at both extremes that was used to clone it into
438 pREC9 using its unique BamHI site, resulting in plasmid pREC17. Finally, the C-terminal
439 His tag from pREC17 was removed by inverse-PCR using oREC50 (5'-
440 TGAGATCCGGCTGCTAACAAAG) and oREC51 (5'-
441 GCGTTTAACCTTAACTTGGCGAGCCA) resulting in pREC28 bearing a spectinomycin
442 cassette for selection in *Synechocystis* and a Bom site for bacterial conjugation of the
443 deletion strain for *apcG*. The phospho-mimicking complementation constructs were
444 generated by inverse-PCR using pREC28 as template with primers oREC38 (5'-
445 CCGGCTCCGGCTGCTGCTAAAAAAACT) and oREC39 (5'-
446 TTTTTCCACCGGAGCTACCTCCG) for the permanent non-phosphorylated version
447 (residues 46-48 TTS into AAA, construct pREC30) and the phospho-mimicking version
448 (residues 46-48 TTS to EEE, construct pREC31) using primers oREC39 and oREC42 (5'-
449 CCGGCTCCGGAAGAAGAAAAAAAAACT).
450 Furthermore, constructs for over-expression in *E. coli* for a truncated version of ApcG
451 removing its PBS binding domain (residues 82 to 121) and keeping a C-terminal His tag
452 was obtained by inverse-PCR using pREC4 as template and primers oREC32 (5'-
453 AACTTTGGCCTTGGGAGCCGGGG) and oREC33 (5'-
454 GGTCTCGAGCACCACCACCAC), to then sub-clone this region using BamHI and NdeI
455 into pBF6 resulting in plasmid pREC54 for tetracycline bacterial induction. Likewise,
456 phosho-mimicking versions for over-expression in *E. coli* were obtained by inverse-PCR
457 using pREC54 as template and primers oREC38 and oREC39 (permanent non-
458 phosphorylated, pREC56) as well as oREC39 and oREC42 (phospho-mimicking version,
459 pREC55). Transformation of wild type as well as the ApcG deletion mutant was performed
460 by bacterial conjugation as described by Black et al. (1993).
461
462 ***Synechocystis* strains genotyping**

463 Cyanobacteria strain cultures were grown to OD_{750} 0.6 – 0.8 under normal conditions and
464 their genomic DNA was extracted by the phenol - chloroform method described by Billi et
465 al. (1998). For amplification of the wild type allele the PCR used primers oREC12 (5'-
466 AGACGGGGAAAAGGCTCTAC) and oREC13 (5'- CCGCTTCAATTTCCTCGTCC).
467 However, the deletion allele was amplified with primers oREC12 and oREC27 (5'-
468 TTCCACGGACTATAGACTATACT). The over-expression insertion was detected by
469 amplifying a fragment using primers oREC57 (5'-
470 CCCAGGGACAATGTGACCAAAAAATTCA) and oCK11 (5'-
471 GCTAGTTATTGCTCAGCGG).
472
473 **Protein expression and purification**
474 Plasmids carrying the truncated form of ApcG for pull-down experiments (pREC54,
475 pREC55 and pREC56) were transformed into *E. coli* BL21 DE3 (Invitrogen, Carlsbad, CA,
476 USA). Cell cultures were grown in luria broth under 37°C till they reached OD_{600} ~ 0.7,
477 followed by induction with 10 µg ml^{-1} anhydrous tetracycline at 25°C overnight. One-liter
478 cultures were centrifuged and resuspended in Buffer A (50 mM Tris pH 8, 200 mM NaCl)
479 with protease inhibitor cocktail (Sigma, St. Louis, MO, USA), DNase I (Sigma) and lysed
480 using two passes through a cell disruptor (Constant Systems, Aberdeenshire, UK) at
481 15 kPSI. The soluble fraction of the lysed sample was obtained by centrifugation for 30
482 min at 30,000 x g and 4°C. The recombinant proteins were purified loading the cell lysate
483 supernatant to a 5 ml HisTrap HP column (GE Healthcare, Little Chalfont, UK), washed
484 with Buffer A, followed by a 5-column volume (CV) of 90% Buffer A and 10% Buffer B
485 (50 mM Tris pH 8, 200 mM NaCl, 500 mM imidazole) and eluted with a 5 CV gradient
486 from 10 to 100% Buffer B. The recombinant proteins were further purified by cation
487 exchange. The eluate from HisTrap was diluted with 50 mM Tris pH 8 10 times to reach
488 20 mM NaCl and loaded into pre-equilibrated cation exchange resin (TOYOPEARL SP-
489 650, column volume 5 ml) and performed the chromatography by gravity at 4°C. The
490 column was then washed with 10 CV of buffer W (50 mM Tris pH 8, 20 mM NaCl), 5 CV
491 with W2 (50 mM Tris pH 8, 50 mM NaCl) and eluted with buffer A. When purifying the
492 truncated form of ApcG with residues 46-48 TSS mutated to EEE (phospho-mimicking),
493 cation exchange step was omitted due to their weak binding to the resin. Protein

494 concentration was measured using BCA method (Pierce BCA Protein Assay Kit, 23227,
495 Thermo Scientific).
496
497 **Pull-down experiments with solubilized thylakoid membranes from *Synechocystis***
498 Cyanobacterial cultures of the *apcG* deletion strain grown for one week under normal
499 conditions were collected by centrifugation and resuspended in 0.1 M phosphate buffer
500 and pH 7.5. The cells were broken by French pressing, and the membranes were
501 separated from the soluble proteins by centrifugating the sample for 30 min and 45,000 x
502 g at 4°C. The thylakoids in the pellet fraction were resuspended in 10 ml of solubilization
503 buffer (1 % dodecyl-beta-D-maltoside, 750 mM aminocaproic acid, 50 mM Bis-Tris pH 7
504 and 50 mM imidazole) and were incubated on ice for 30 min. After this the sample was
505 centrifuged for 30 min at 30,000 x g at 4°C to discard insoluble membrane complexes.
506 The soluble fraction corresponds to the solubilized thylakoid super-complexes whose
507 protein and chlorophyll contents were quantified by BCA method and methanol extraction
508 respectively. The solubilized thylakoid super-complexes were loaded into NTA nickel
509 beads (0.8 ml column volume) pre-incubated with the truncated ApcG with His tag at its
510 C-terminus in solubilization buffer with 50 mM imidazole. Beads were incubated under
511 rotation for 1 hour at 4°C. The beads were then centrifuged for 2 min at 100 x g and the
512 supernatant discarded to wash the beads 4 times with 10 CV of solubilization buffer and
513 50 mM imidazole. The elution was performed with 1.5 ml of solubilization buffer and 200
514 mM imidazole.
515
516 **Separation of super-complexes in first dimension native and second dimension**
517 **denaturing gels**
518 Solubilized thylakoid super-complexes as well as eluates from pull-down experiments
519 were separated in native gels following the method described by Schagger and Vonjagow
520 (1991). For clear native gels though, the same method described by Schagger and
521 Vonjagow (1991) was followed but preparing the cathode running buffer as well as the
522 sample loading buffer without Coomassie brilliant blue. After the separation of super-
523 complexes in native gels, we further separated their protein content in a second

524 dimension under denaturing conditions with 12% SDS-polyacrylamide gels supplemented
525 with 4 M urea. The gels were stained using the method described by Blum et al. (1987).
526
527 **Preparation of total protein extracts**
528 *Synechocystis* strains were grown in 10 ml BG-11 media in flasks of 25 ml under agitation
529 under constant light (c. 25–30 µmol photons m^{-2} s^{-1}) supplemented with 3% CO_2 until
530 they reached OD_{750} ~ 1. Cultures were centrifuged and the supernatant discarded to
531 resuspend cells in extraction buffer (50 mM HEPES pH 7.0, 25 mM $CaCl_2$, 5 mM $MgCl_2$,
532 10% [v/v] glycerol and protease inhibitor cocktail). Resuspended cells were broken by
533 French pressing, and Triton X-100 was added to a final concentration of 1 % (v/v). After
534 incubation on ice for 10 minutes, cell debris was discarded by centrifugation for 2 minutes
535 at 2.000 g, 4°C and the supernatant rescued as total protein extract. Protein concentration
536 was measured by BCA method.
537
538 **Cyanobacterial pigment analyses**
539 To quantify chlorophyll and carotenoids, 1 mL culture was harvested in an Eppendorf
540 tube. The cell pellet was suspended in 100% methanol, and absorption spectra of the
541 extracted pigments were measured. The pigment concentration was calculated using
542 calculations described by Zavřel (2015). Phycobiliproteins were quantified as described
543 by Zavrel et al. (2018).
544
545 **Immunoblot analyses**
546 Proteins separated into SDS-PAGE gels were transferred to a nitrocellulose membrane
547 (Amersham™, Protran®). The membrane was blocked with 5% milk in TBS (Tris 20 mM
548 and 150 mM NaCl) at room temperature for one hour then incubated with monospecific
549 polyclonal antisera in TBS-T (Tris 20 mM, 150 mM NaCl and 0.01% tween-20) overnight
550 at 4°C (anti-PsbA; AS05 084A; anti-PsaB; AS10 695; anti-APC; AS08 277; Agrisera, anti-
551 His tag; TA150087; OriGene). The membrane was washed 3 times in TBST-T at room
552 temperature for 15 minutes each wash followed by incubation with secondary polyclonal
553 anti-rabbit antisera HRP for one hour at room temperature in TBS-T (Jackson

554 ImmunoResearch, 111-035-003). After 3 additional washes with TBS-T, the membrane
555 was visualized by the enhanced chemiluminescence technique.
556
557 **Isolation of PBSs from *Synechocystis***
558 Cyanobacteria cultures of one liter were grown under normal conditions for one week and
559 harvested for resuspension in phosphate buffer (0.8 M, pH 7.5) supplemented with
560 protease inhibitor cocktail (Sigma, St. Louis, MO, USA). Cells were broken by French
561 pressing followed by the addition of 1% Triton X-100 and an incubation of 15 min at room
562 temperature under darkness and gentle rotation. The soluble fraction containing PBSs
563 was separated from the membrane fraction by centrifugation for 30 min at 30,000 x g and
564 room temperature. The supernatant was rescued and centrifuged again for one hour at
565 42,000 x g and room temperature and the dark blue supernatant was separated from the
566 green top with a syringe. These samples were loaded onto sucrose gradients composed
567 of 1.5 M, 1 M, 0.75 M, 0.5 M and 0.25 M phases in phosphate buffer (0.8 M, pH 7.5), and
568 separated by centrifugation at 25,000 rpm and room temperature overnight. Intact PBS
569 fractions were recovered from the 0.75 M - 1 M interface of the sucrose gradients. The
570 PBS protein content was measured by BCA method and proteins precipitated by
571 trichloroacetic acid before being separated into SDS-PAGE.
572
573 **Measurements of absorption or fluorescence spectra**
574 Whole-cells or PBS absorption spectra were recorded with a Varian Cary Bio 100
575 spectrophotometer (Agilent). Fluorescence spectra of isolated PBS samples were
576 recorded with a fluorimeter (SpectraMax M2, Molecular Devices) exciting at 590 nm and
577 emission spectra collected at room temperature from 610 to 800 nm.
578
579 **Fluorescence emission spectroscopy at 77 K**
580 Whole cell fluorescence spectra were obtained from cells grown in BG-11 media enriched
581 with 3% CO_2 at an OD_{720} of 0.5 - 0.8. Cells were diluted for a final glycerol concentration
582 of 60% and an absorption at 430 nm no higher than 0.1. Cells were dark incubated at
583 room temperature for 15 minutes and brought to 77K for 15 minutes prior every
584 measurement. Fluorescence emission was recorded at 77K using a home-built

585 spectrometer (Gurchiek et al., 2020) with LED compact double monochromator for
586 excitation light source and a cryogenic chamber optistat DN (Oxford instruments). The
587 excitation wavelength was 430 or 590 nm with a 2-nm slit size. The emission wavelength
588 measured was from 600 to 800 nm with a 4-nm slit size.
589 For state transitions measurements, cells were grown in BG-11 supplemented with 20
590 mM $NaHCO_3$ and 10 mM HEPES-NaOH (pH 8.0) on a shaker at 30°C under constant
591 light intensity at ~50 µmol photons m^{-2} s^{-1}. The cell concentration was adjusted to OD_{630}
592 of 0.2-0.3 as measured by absorption spectroscopy using an integrating sphere
593 (Shimadzu UV-3600i Plus with ISR-603). The dark treatment was applied for 20 min to
594 induce State II and subsequently, the blue light illumination was applied for 10 min to
595 induce State I (Bhatti et al., 2020, Calzadilla and Kirilovsky, 2020, McConnell et al., 2002).
596 Fluorescence emission was recorded at 77 K using a FluoroMax-4 spectrofluorometer
597 (Horiba Scientific). The excitation wavelength was 590 nm with a 2-nm slit size. The
598 emission wavelength measured was from 630 to 780 nm with a 2-nm slit size.
599 Fluorescence emission for each sample was recorded consecutively three times to obtain
600 averaged spectra. The results shown are averages of three independent biological
601 replicates.
602
603 **Software**
604 Figures were generated using Adobe Illustrator CS6. Graphs and statistical analyses
605 were done using Python (Sanner, 1999) and GraphPad Prism version 6.0 (GraphPad
606 Software, La Jolla, CA, USA) (www.graphpad.com). Structural figures were prepared with
607 PyMOL (www.pymol.org). The sequence conservation logo was generated with Weblogo
608 (Crooks et al., 2004).
609
610 **Acknowledgments and funding**
611 The research in the Kerfeld lab was supported by the Office of Science of the U.S.
612 Department of Energy under award number DE-SC0020606. M.I. and K.K.N. were
613 supported by the U.S. Department of Energy, Office of Science, Basic Energy Sciences,
614 Chemical Sciences, Geosciences, and Biosciences Division under field work proposal
615 449B. K.K.N. is an investigator of the Howard Hughes Medical Institute. The authors

616 greatly thank Dr. Warren Beck (MSU) for facilitating the instruments for 77K fluorescence
617 spectra measurements.
618

619 **Author Contributions**

620 R.E-C. designed and conducted the research, analyzed the data, and wrote the article,
621 M.I. conducted low temperature fluorescence and analyzed the data, T.Z. conducted
622 cyanobacteria growth experiments and analyzed data, S.L-Y. conducted pigment
623 analyses of cyanobacteria strains and analyzed data, C.A.K. and M.S. designed research,
624 analyzed the data and wrote the article. J.C., K.K.N. as well as all other authors provided
625 comments on the manuscript and contributed to experimental design.
626

627 **Conflict of interests**

628 The authors declare that they have no conflicts of interest with the contents of this
629 article.
630

631 **REFERENCES**

632

633 ADIR, N. 2005. Elucidation of the molecular structures of components of the
634 phycobilisome: reconstructing a giant. *Photosynthesis Research,* 85**,** 15-32.
635 ANDERSON, L. K. & TOOLE, C. M. 1998. A model for early events in the assembly
636 pathway of cyanobacterial phycobilisomes. *Molecular Microbiology,* 30**,** 467-474.
637 ANGELERI, M., MUTH-PAWLAK, D., ARO, E. M. & BATTCHIKOVA, N. 2016. Study of
638 O-Phosphorylation Sites in Proteins Involved in Photosynthesis-Related
639 Processes in Synechocystis sp. Strain PCC 6803: Application of the SRM
640 Approach. *J Proteome Res,* 15**,** 4638-4652.
641 BECKOVA, M., GARDIAN, Z., YU, J., KONIK, P., NIXON, P. J. & KOMENDA, J. 2017.
642 Association of Psb28 and Psb27 Proteins with PSII-PSI Supercomplexes upon
643 Exposure of Synechocystis sp. PCC 6803 to High Light. *Mol Plant,* 10**,** 62-72.
644 BHATTI, A. F., CHOUBEH, R. R., KIRILOVSKY, D., WIENTJES, E. & VAN
645 AMERONGEN, H. 2020. State transitions in cyanobacteria studied with
646 picosecond fluorescence at room temperature. *Biochimica Et Biophysica Acta-*
647 *Bioenergetics,* 1861.
648 BIBBY, T. S., NIELD, J. & BARBER, J. 2001a. Iron deficiency induces the formation of
649 an antenna ring around trimeric photosystem I in cyanobacteria. *Nature,* 412**,** 743-
650 5.
651 BIBBY, T. S., NIELD, J. & BARBER, J. 2001b. Three-dimensional model and
652 characterization of the iron stress-induced CP43'-photosystem I supercomplex

653 isolated from the cyanobacterium Synechocystis PCC 6803. *J Biol Chem,* 276**,**
654 43246-52.
655 BILLI, D., CAIOLA, M. G., PAOLOZZI, L. & GHELARDINI, P. 1998. A method for DNA
656 extraction from the desert cyanobacterium Chroococcidiopsis and its application
657 to identification of ftsZ. *Applied and Environmental Microbiology,* 64**,** 4053-4056.
658 BLACK, T. A., CAI, Y. P. & WOLK, C. P. 1993. Spatial Expression and Autoregulation of
659 Hetr, a Gene Involved in the Control of Heterocyst Development in Anabaena (Vol
660 9, Pg 77, 1993). *Molecular Microbiology,* 10**,** 1153-1153.
661 BLUM, H., BEIER, H. & GROSS, H. J. 1987. Improved Silver Staining of Plant-Proteins,
662 Rna and DNA in Polyacrylamide Gels. *Electrophoresis,* 8**,** 93-99.
663 BONAVENTURA, C. & MYERS, J. 1969. Fluorescence and Oxygen Evolution from
664 Chlorella Pyrenoidosa. *Biochimica Et Biophysica Acta,* 189**,** 366-+.
665 BRYANT, D. A., GUGLIELMI, G., DE MARSAC, N. T., CASTETS, A. & COHEN-BAZIRE,
666 G. 1979. The structure of cyanobacterial phycobilisomes: a model. *Archives of*
667 *Microbiology,* 123**,** 113–127.
668 BURNAP, R. L., TROYAN, T. & SHERMAN, L. A. 1993. The highly abundant chlorophyll-
669 protein complex of iron-deficient Synechococcus sp. PCC7942 (CP43') is encoded
670 by the isiA gene. *Plant Physiol,* 103**,** 893-902.
671 CALZADILLA, P. I. & KIRILOVSKY, D. 2020. Revisiting cyanobacterial state transitions.
672 *Photochemical & Photobiological Sciences,* 19**,** 585-603.
673 CHEN, Z., ZHAN, J., CHEN, Y., YANG, M., HE, C., GE, F. & WANG, Q. 2015. Effects of
674 Phosphorylation of beta Subunits of Phycocyanins on State Transition in the Model
675 Cyanobacterium Synechocystis sp. PCC 6803. *Plant Cell Physiol,* 56**,** 1997-2013.
676 CHO, S. H., JEONG, Y., HONG, S. J., LEE, H., CHOI, H. K., KIM, D. M., LEE, C. G.,
677 CHO, S. & CHO, B. K. 2021. Different Regulatory Modes of Synechocystis sp.
678 PCC 6803 in Response to Photosynthesis Inhibitory Conditions. *mSystems,* 6**,**
679 e0094321.
680 CROOKS, G. E., HON, G., CHANDONIA, J. M. & BRENNER, S. E. 2004. WebLogo: A
681 sequence logo generator. *Genome Research,* 14**,** 1188-1190.
682 CUNNINGHAM, F. X., TICE, A. B., PHAM, C. & GANTT, E. 2010. Inactivation of Genes
683 Encoding Plastoglobulin-Like Proteins in Synechocystis sp PCC 6803 Leads to a
684 Light-Sensitive Phenotype. *Journal of Bacteriology,* 192**,** 1700-1709.
685 DE MARSAC, N. T. & COHEN-BAZIRE, G. 1977. Molecular composition of
686 cyanobacterial phycobilisomes. *Proc Natl Acad Sci U S A,* 74**,** 1635-9.
687 DOMINGUEZ-MARTIN, M. A., SAUER, P. V., KIRST, H., SUTTER, M., BINA, D.,
688 GREBER, B. J., NOGALES, E., POLIVKA, T. & KERFELD, C. A. 2022. Structures
689 of a phycobilisome in light-harvesting and photoprotected states. *Nature*.
690 DONG, C. X., TANG, A. H., ZHAO, J. D., MULLINEAUX, C. W., SHEN, G. Z. & BRYANT,
691 D. A. 2009. ApcD is necessary for efficient energy transfer from phycobilisomes to
692 photosystem I and helps to prevent photoinhibition in the cyanobacterium
693 Synechococcus sp PCC 7002. *Biochimica Et Biophysica Acta-Bioenergetics,*
694 1787**,** 1122-1128.
695 DUHRING, U., AXMANN, I. M., HESS, W. R. & WILDE, A. 2006. An internal antisense
696 RNA regulates expression of the photosynthesis gene isiA. *Proc Natl Acad Sci U*
697 *S A,* 103**,** 7054-8.

EMLYN-JONES, D., ASHBY, M. K. & MULLINEAUX, C. W. 1999. A gene required for the regulation of photosynthetic light harvesting in the cyanobacterium Synechocystis 6803. *Molecular Microbiology,* 33**,** 1050-1058.

ENGLUND, E., LIANG, F. Y. & LINDBERG, P. 2016. Evaluation of promoters and ribosome binding sites for biotechnological applications in the unicellular cyanobacterium Synechocystis sp PCC 6803. *Scientific Reports,* 6.

FOLEA, I. M., ZHANG, P., ARO, E. M. & BOEKEMA, E. J. 2008. Domain organization of photosystem II in membranes of the cyanobacterium Synechocystis PCC6803 investigated by electron microscopy. *FEBS Lett,* 582**,** 1749-54.

FUENTE, D., LAZAR, D., OLIVER-VILLANUEVA, J. V. & URCHUEGUIA, J. F. 2021. Reconstruction of the absorption spectrum of Synechocystis sp. PCC 6803 optical mutants from the in vivo signature of individual pigments. *Photosynth Res,* 147**,** 75-90.

GANTT, E. & CONTI, S. F. 1969. Ultrastructure of blue-green algae. *J Bacteriol,* 97**,** 1486-93.

GINDT, Y. M., ZHOU, J. H., BRYANT, D. A. & SAUER, K. 1992. Core Mutations of Synechococcus Sp Pcc-7002 Phycobilisomes - a Spectroscopic Study. *Journal of Photochemistry and Photobiology B-Biology,* 15**,** 75-89.

GLAUSER, M., BRYANT, D. A., FRANK, G., WEHRLI, E., RUSCONI, S. S., SIDLER, W. & ZUBER, H. 1992. Phycobilisome Structure in the Cyanobacteria Mastigocladus-Laminosus and Anabaena Sp Pcc-7120. *European Journal of Biochemistry,* 205**,** 907-915.

GURCHIEK, J. K., ROSE, J. B., GUBERMAN-PFEFFER, M. J., TILLUCK, R. W., GHOSH, S., GASCON, J. A. & BECK, W. F. 2020. Fluorescence Anisotropy Detection of Barrier Crossing and Ultrafast Conformational Dynamics in the S(2) State of beta-Carotene. *J Phys Chem B,* 124**,** 9029-9046.

HAVAUX, M., GUEDENEY, G., HE, Q. F. & GROSSMAN, A. R. 2003. Elimination of high-light-inducible polypeptides related to eukaryotic chlorophyll a/b-binding proteins results in aberrant photoacclimation in Synechocystis PCC6803. *Biochimica Et Biophysica Acta-Bioenergetics,* 1557**,** 21-33.

HODGES, M. & BARBER, J. 1983. State 1-State 2 Transitions in a Unicellular Green Algae : Analysis of In Vivo Chlorophyll Fluorescence Induction Curves in the Presence of 3-(3,4-Dichlorophenyl)-1, 1-dimethylurea (DCMU). *Plant Physiol,* 72**,** 1119-22.

JUMPER, J., EVANS, R., PRITZEL, A., GREEN, T., FIGURNOV, M., RONNEBERGER, O., TUNYASUVUNAKOOL, K., BATES, R., ZIDEK, A., POTAPENKO, A., BRIDGLAND, A., MEYER, C., KOHL, S. A. A., BALLARD, A. J., COWIE, A., ROMERA-PAREDES, B., NIKOLOV, S., JAIN, R., ADLER, J., BACK, T., PETERSEN, S., REIMAN, D., CLANCY, E., ZIELINSKI, M., STEINEGGER, M., PACHOLSKA, M., BERGHAMMER, T., BODENSTEIN, S., SILVER, D., VINYALS, O., SENIOR, A. W., KAVUKCUOGLU, K., KOHLI, P. & HASSABIS, D. 2021. Highly accurate protein structure prediction with AlphaFold. *Nature,* 596**,** 583-589.

KERFELD, C. A., MELNICKI, M. R., SUTTER, M. & DOMINGUEZ-MARTIN, M. A. 2017. Structure, function and evolution of the cyanobacterial orange carotenoid protein and its homologs. *New Phytol,* 215**,** 937-951.

LAGARDE, D., BEUF, L. & VERMAAS, M. 2000. Increased production of zeaxanthin and other pigments by application of genetic engineering techniques to Synechocystis sp strain PCC 6803. *Applied and Environmental Microbiology,* 66**,** 64-72.

LEVERENZ, R. L., SUTTER, M., WILSON, A., GUPTA, S., THUROTTE, A., DE CARBON, C. B., PETZOLD, C. J., RALSTON, C., PERREAU, F., KIRILOVSKY, D. & KERFELD, C. A. 2015. A 12 angstrom carotenoid translocation in a photoswitch associated with cyanobacterial photoprotection. *Science,* 348**,** 1463-1466.

LI, D., XIE, J., ZHAO, J., XIA, A., LI, D. & GONG, Y. 2004. Light-induced excitation energy redistribution in Spirulina platensis cells: "spillover" or "mobile PBSs"? *Biochim Biophys Acta,* 1608**,** 114-21.

LI, H., LI, D., YANG, S., XIE, J. & ZHAO, J. 2006. The state transition mechanism - simply depending on light-on and -off in Spirulina platensis. *Biochim Biophys Acta,* 1757**,** 1512-9.

LI, M. J., MA, J. F., LI, X. M. & SUI, S. F. 2021. In situ cryo-ET structure of phycobilisome-photosystem II supercomplex from red alga. *Elife,* 10.

LIU, H. 2023. Cyanobacterial Phycobilisome Allostery as Revealed by Quantitative Mass Spectrometry. *Biochemistry,* 62**,** 1307-1320.

LIU, H. J., ZHANG, H., NIEDZWIEDZKI, D. M., PRADO, M., HE, G. N., GROSS, M. L. & BLANKENSHIP, R. E. 2013. Phycobilisomes Supply Excitations to Both Photosystems in a Megacomplex in Cyanobacteria. *Science,* 342**,** 1104-1107.

LUIMSTRA, V. M., SCHUURMANS, J. M., HELLINGWERF, K. J., MATTHIJS, H. C. P. & HUISMAN, J. 2020. Blue light induces major changes in the gene expression profile of the cyanobacterium Synechocystis sp. PCC 6803. *Physiol Plant,* 170**,** 10-26.

MAEDA, H., SAKURAGI, Y., BRYANT, D. A. & DELLAPENNA, D. 2005. Tocopherols protect Synechocystis sp strain PCC 6803 from lipid peroxidation. *Plant Physiology,* 138**,** 1422-1435.

MCCONNELL, M. D., KOOP, R., VASIL'EV, S. & BRUCE, D. 2002. Regulation of the distribution of chlorophyll and phycobilin-absorbed excitation energy in cyanobacteria. A structure-based model for the light state transition. *Plant Physiol,* 130**,** 1201-12.

MULLINEAUX, C. W. 2014. Electron transport and light-harvesting switches in cyanobacteria. *Front Plant Sci,* 5**,** 7.

MULLINEAUX, C. W., TOBIN, M. J. & JONES, G. R. 1997. Mobility of photosynthetic complexes in thylakoid membranes. *Nature,* 390**,** 421-424.

NAGAO, R., KATO, K., HAMAGUCHI, T., UENO, Y., TSUBOSHITA, N., SHIMIZU, S., FURUTANI, M., EHIRA, S., NAKAJIMA, Y., KAWAKAMI, K., SUZUKI, T., DOHMAE, N., AKIMOTO, S., YONEKURA, K. & SHEN, J. R. 2023. Structure of a monomeric photosystem I core associated with iron-stress-induced-A proteins from Anabaena sp. PCC 7120. *Nat Commun,* 14**,** 920.

NIEVES-MORION, M., LECHNO-YOSSEF, S., LOPEZ-IGUAL, R., FRIAS, J. E., MARISCAL, V., NURNBERG, D. J., MULLINEAUX, C. W., WOLK, C. P. & FLORES, E. 2017. Specific Glucoside Transporters Influence Septal Structure and Function in the Filamentous, Heterocyst-Forming Cyanobacterium Anabaena sp. Strain PCC 7120. *J Bacteriol,* 199.

789 OLIVE, J., AJLANI, G., ASTIER, C., RECOUVREUR, M. & VERNOTTE, C. 1997.
790 Ultrastructure and light adaptation of phycobilisome mutants of Synechocystis
791 PCC 6803. *Biochimica Et Biophysica Acta-Bioenergetics,* 1319**,** 275-282.
792 PENG, P. P., DONG, L. L., SUN, Y. F., ZENG, X. L., DING, W. L., SCHEER, H., YANG,
793 X. J. & ZHAO, K. H. 2014. The structure of allophycocyanin B from Synechocystis
794 PCC 6803 reveals the structural basis for the extreme redshift of the terminal
795 emitter in phycobilisomes. *Acta Crystallographica Section D-Structural Biology,* 70**,**
796 2558-2569.
797 PLATT, T., GALLEGOS, C. L. & HARRISON, W. G. 1980. Photoinhibition of
798 Photosynthesis in Natural Assemblages of Marine-Phytoplankton. *Journal of*
799 *Marine Research,* 38**,** 687-701.
800 RAST, A., SCHAFFER, M., ALBERT, S., WAN, W., PFEFFER, S., BECK, F., PLITZKO,
801 J. M., NICKELSEN, J. & ENGEL, B. D. 2019. Biogenic regions of cyanobacterial
802 thylakoids form contact sites with the plasma membrane. *Nature Plants,* 5**,** 436-
803 446.
804 RIPPKA, R., DERUELLES, J., WATERBURY, J. B., HERDMAN, M. & STANIER, R. Y.
805 1979. Generic Assignments, Strain Histories and Properties of Pure Cultures of
806 Cyanobacteria. *Journal of General Microbiology,* 111**,** 1-61.
807 SANNER, M. F. 1999. Python: A programming language for software integration and
808 development. *Journal of Molecular Graphics & Modelling,* 17**,** 57-61.
809 SARCINA, M., TOBIN, M. J. & MULLINEAUX, C. W. 2001. Diffusion of phycobilisomes
810 on the thylakoid membranes of the cyanobacterium Synechococcus 7942 - Effects
811 of phycobilisome size, temperature, and membrane lipid composition. *Journal of*
812 *Biological Chemistry,* 276**,** 46830-46834.
813 SCHAFER, L., VIOQUE, A. & SANDMANN, G. 2005. Functional in situ evaluation of
814 photosynthesis-protecting carotenoids in mutants of the cyanobacterium
815 Synechocystis PCC6803. *J Photochem Photobiol B,* 78**,** 195-201.
816 SCHAGGER, H. & VONJAGOW, G. 1991. Blue Native Electrophoresis for Isolation of
817 Membrane-Protein Complexes in Enzymatically Active Form. *Analytical*
818 *Biochemistry,* 199**,** 223-231.
819 STRASKOVA, A., STEINBACH, G., KONERT, G., KOTABOVA, E., KOMENDA, J.,
820 TICHY, M. & KANA, R. 2019. Pigment-protein complexes are organized into stable
821 microdomains in cyanobacterial thylakoids. *Biochimica Et Biophysica Acta-*
822 *Bioenergetics,* 1860.
823 TOYOSHIMA, M., TOKUMARU, Y., MATSUDA, F. & SHIMIZU, H. 2020. Assessment of
824 Protein Content and Phosphorylation Level in Synechocystis sp. PCC 6803 under
825 Various Growth Conditions Using Quantitative Phosphoproteomic Analysis.
826 *Molecules,* 25.
827 XU, X. L., YANG, S. Z., XIE, J. & ZHAO, J. Q. 2012. Kinetics and dynamics for light state
828 transition in cyanobacterium Spirulina platensis cells. *Biochemical and Biophysical*
829 *Research Communications,* 422**,** 233-237.
830 YANG, S. Z., SU, Z. Q., LI, H., FENG, J. J., XIE, J., XIA, A. D., GONG, Y. D. & ZHAO, J.
831 Q. 2007. Demonstration of phycobilisome mobility by the time- and space-
832 correlated fluorescence imaging of a cyanobacterial cell. *Biochimica Et Biophysica*
833 *Acta-Bioenergetics,* 1767**,** 15-21.

YOU, X., ZHANG, X., CHENG, J., XIAO, Y., MA, J., SUN, S., ZHANG, X., WANG, H. W. & SUI, S. F. 2023. In situ structure of the red algal phycobilisome-PSII-PSI-LHC megacomplex. *Nature*.

ZAVREL, T., CHMELIK, D., SINETOVA, M. A. & CERVENY, J. 2018. Spectrophotometric Determination of Phycobiliprotein Content in Cyanobacterium Synechocystis. *J Vis Exp*.

ZAVREL, T., FAIZI, M., LOUREIRO, C., POSCHMANN, G., STUHLER, K., SINETOVA, M., ZORINA, A., STEUER, R. & CERVENY, J. 2019. Quantitative insights into the cyanobacterial cell economy. *Elife,* 8.

ZAVŘEL, T. S., M; J. ČERVENÝ, J. 2015. Measurement of Chlorophyll a and Carotenoids Concentration in Cyanobacteria. *Bio-protocol* 5.

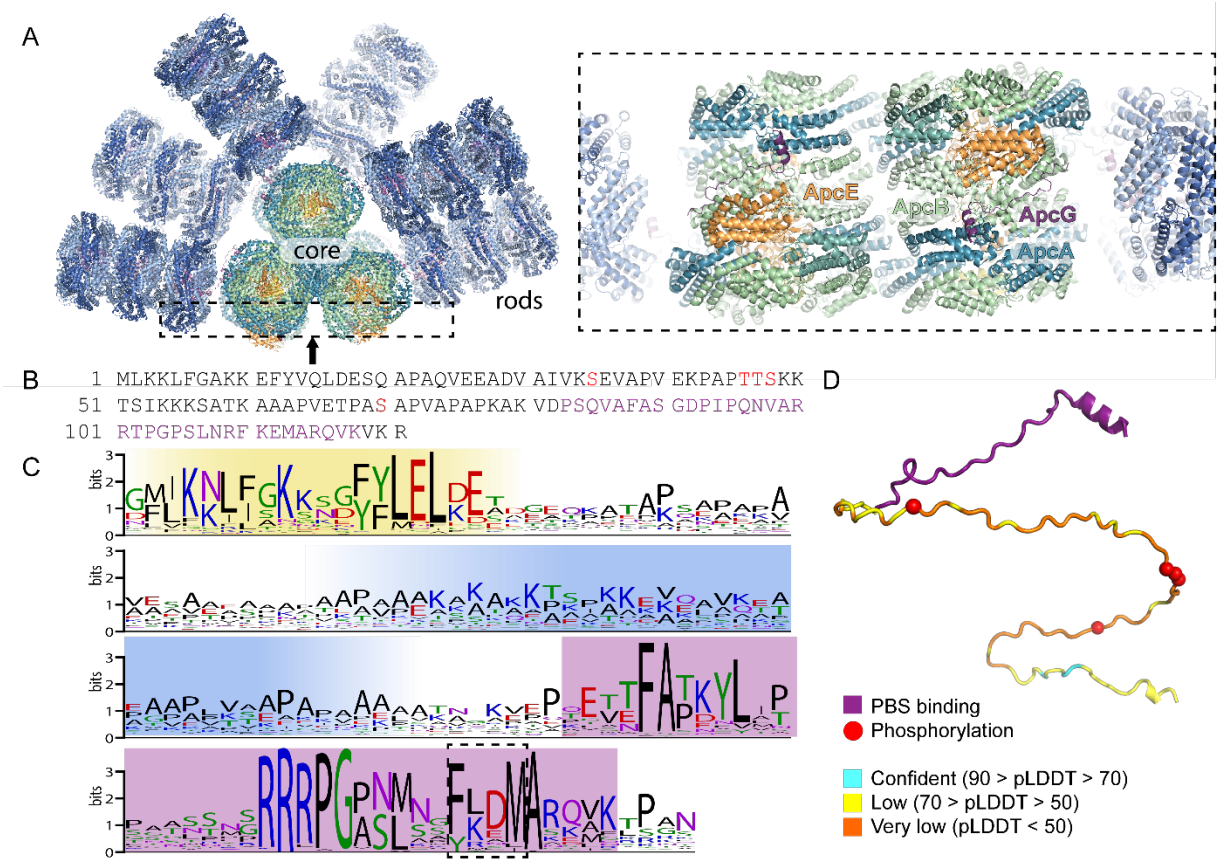

Figure 1. PBS linker protein ApcG binding site, conservation and domain structure. (A) Overview of *Synechocystis* PBS (left) and zoomed in view of ApcG binding site at the bottom cylinder (right). **(B)** Primary structure of *Synechocystis* ApcG. Phosphorylation sites are highlighted in red while PBS binding region is in purple. **(C)** Sequence conservation logo of 347 cyanobacterial ApcG homologs. The N-terminal conserved region is highlighted in yellow, positively charged region in blue and C-terminal PBS binding region in purple. The conserved FxxM motif is highlighted with a dashed box. **(D)** AlphaFold predicted structure (colored according to prediction confidence) of residues 1-121 of ApcG (not present in the cryoEM structure) of the combined with model of the PBS interaction domain from the cryo-EM structure (purple). Phosphorylation sites are shown as red spheres.

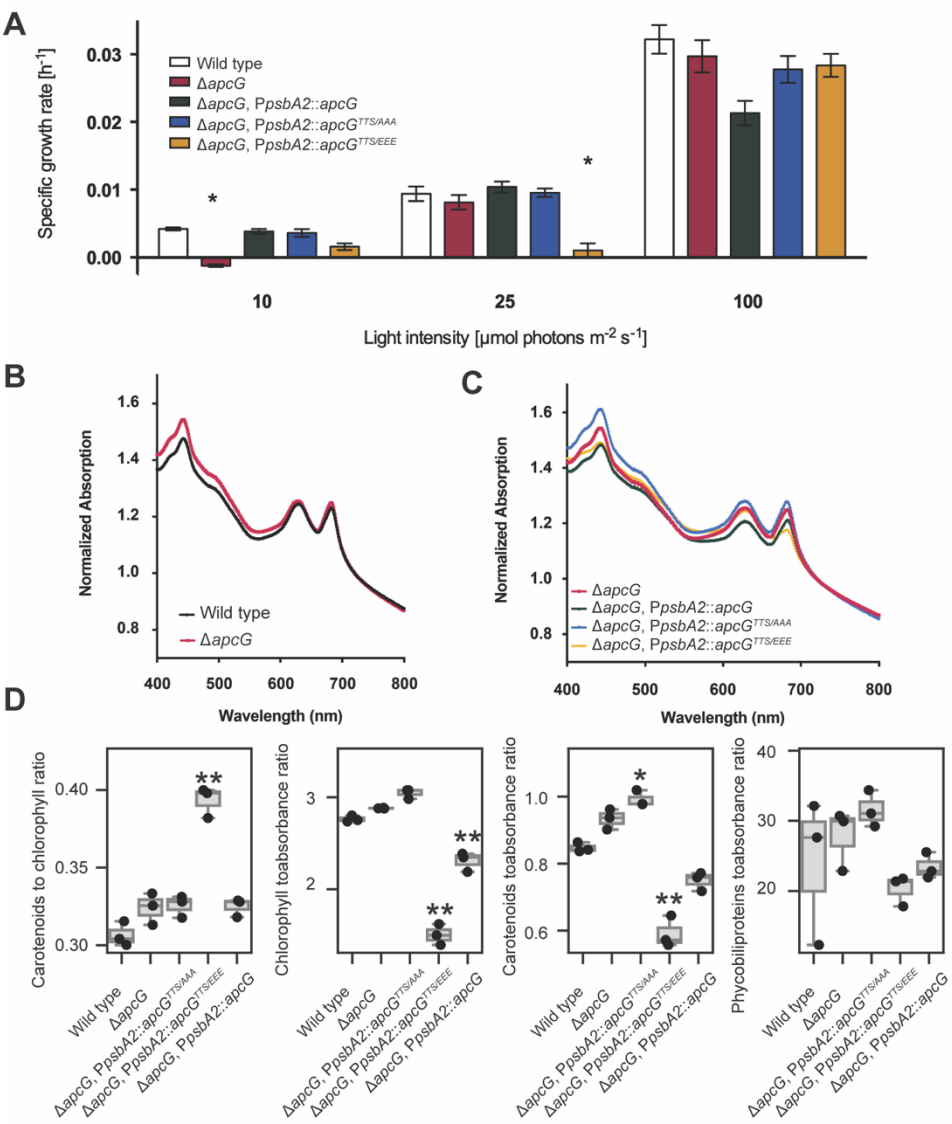

Figure 2. Impact on growth in *apcG* deletion strains. (A) Specific growth rate comparison of the *apcG* deletion, complementation strains and wild type under 10, 25 and 100 µmol photons $m^{-2} \cdot s^{-1}$. Values represent means of four independent replicates ± standard error of mean and asterisks show statistical difference compared to wild type according to Student's *t* test (two-sided, $P < 0.05$). **(B)** Whole-cell absorption spectra for wild type *Synechocystis* and *apcG* deletion mutant, **(C)** and for *apcG* deletion and its complementation strains. Values correspond to averages of three biological replicates normalized to 720 nm. **(D)** Comparison of the relative pigment composition among *apcG* strains. Pigment concentrations were measured in three biological replicates in µg / mL units, and culture turbidity was measured as absorbance at 720 nm. A single asterisk represents statistical significance at *P* value of 0.05, and two asterisks represent statistical difference at *P* value of 0.01.

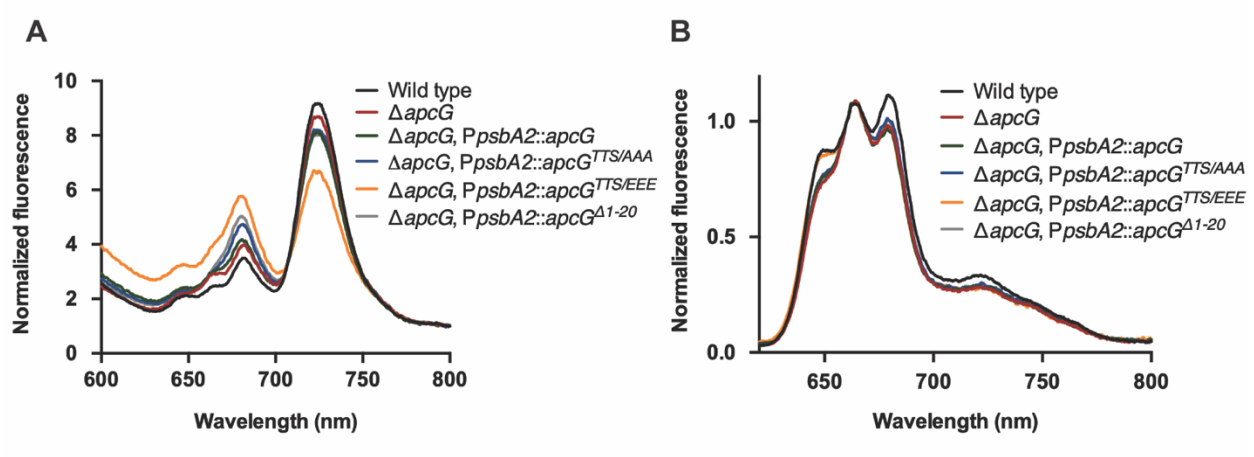

Figure 3. *apcG* deletion and phosphorylation impacts PSII and PSI energy balance. *Synechocystis* cultures were grown to compare their fluorescence under low temperature (77 K). Each curve on the spectra represents the mean from three biological replicates. All cultures were pre-incubated at room temperature in darkness for 15 min before measurements. **(A)** Fluorescence emission spectra of chlorophyll from *Synechocystis* with an excitation of 430 nm. The first peak at 680 nm corresponds to the fluorescence from PSII while the one around 720 nm to PSI. Values correspond to mean of three biological replicates while normalizing the data to 800 nm. **(B)** Fluorescence emission spectra of *Synechocystis* strains by exciting PBS at 590 nm. The fluorescence peak at 650-660 nm correspond to PBS, 680 nm to PSII and 720 nm to PSI. Values correspond to the means of three biological replicates while normalizing the data to the peak of PBS at 660 nm.

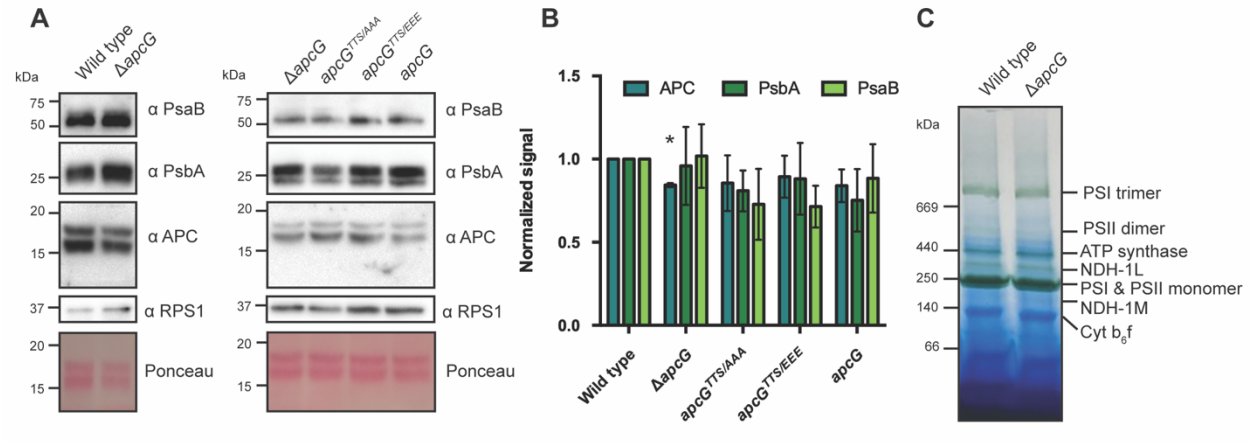

Figure 4. Impact of ApcG deletion on thylakoid super-complexes in *Synechocystis*. (A) Whole-cell protein extracts were obtained from *Synechocystis* strains to compare the accumulation of marker proteins for PBS (APC), PSI (PsaB) and PSII (PsbA). The ribosomal protein RPS1 was used as loading control. A total of 20 µg of protein were loaded for each lane. A representative immunoblot out of three biological replicates is shown. **(B)** Western blot signal quantification from three biological replicates for marker proteins APC, PsbA and PsaB. Values were normalized using the wild type signal. Error bars represent standard error of mean and asterisks represent statistical difference compared to wild type according to Student's *t* test (two-sided, $P < 0.05$)**. (C)** Thylakoid membrane fractions from wild type and *apcG* deletion mutant were solubilized and separated on blue native gels to analyze the accumulation of the major thylakoid super-complexes. A total of 30 µg of chlorophyll were loaded for each strain. A representative native gel from one of three biological replicates is shown.

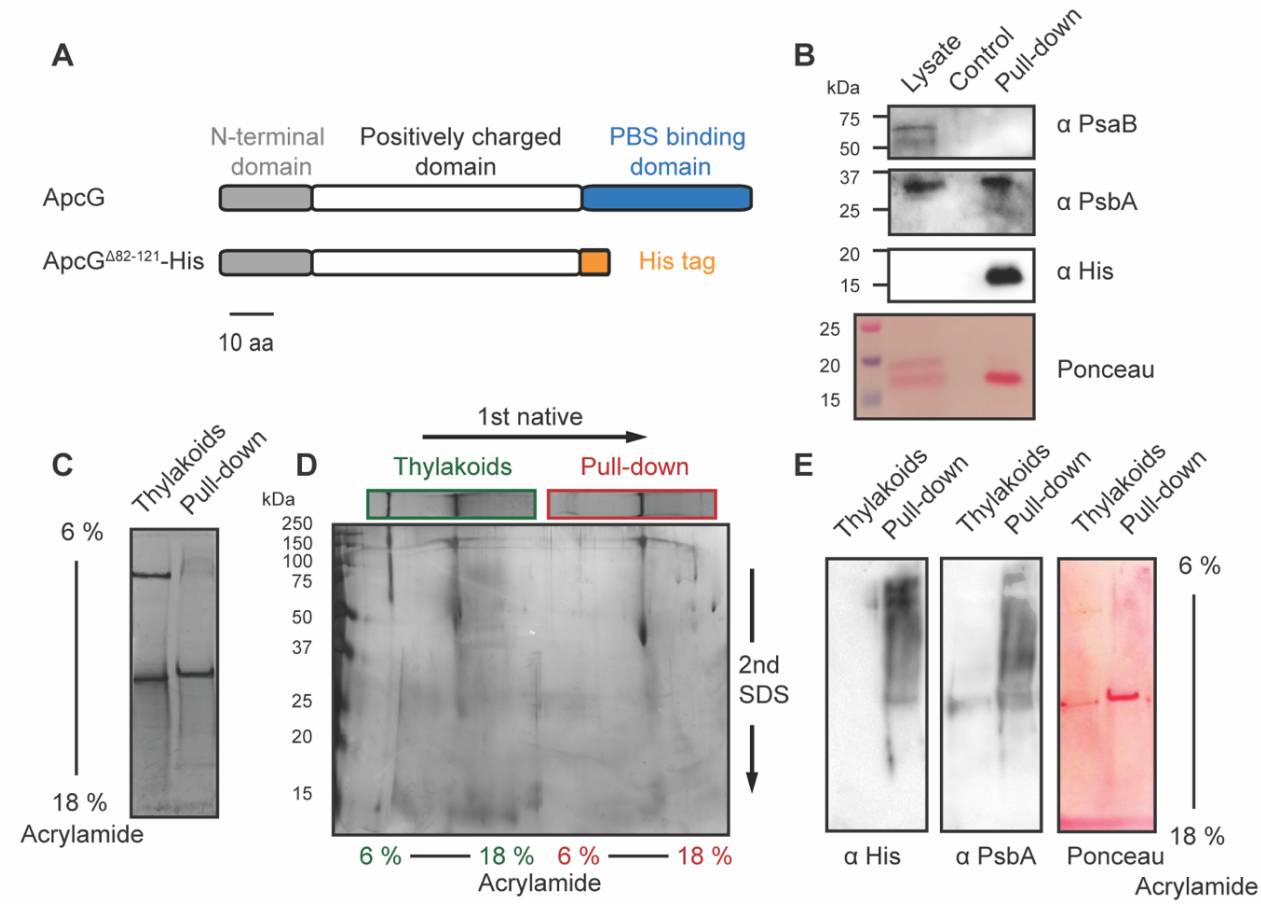

Figure 5. The N-terminal domain of ApcG interacts specifically with PSII. (A) Schematic representation of ApcG domains and the ApcG truncation used for pull-down experiments. **(B)** Immunoblots of the pull-down eluate using antibodies to detect the presence of PSI (anti-PsaB) and PSII (anti-PsbA). Whole-cell protein extract was used as a positive control for marker proteins. **(C)** Solubilized thylakoid membranes were incubated with nickel beads containing ApcG$^{\Delta 82\text{-}121}$-His. After washing the beads and eluting with 200 mM imidazole, the eluate was separated in CN gels. For comparison, solubilized thylakoid membranes were loaded alongside the eluate from the pull-down experiment. A total of 1.3 µg of chlorophyll was loaded into each lane. **(D)** Second dimension of CN gel lanes by SDS-PAGE and stained with silver staining. **(E)** Immunoblots of the first CN gel dimension of pull-down eluate with total thylakoid super-complexes. Antibodies against His-tag were used to detect the presence of ApcG$^{\Delta 82\text{-}121}$-His. Additionally, antibodies against PsbA were used as a marker for PSII. Images from section **(B)** to **(E)** correspond to a representative experiment from three biological replicates.

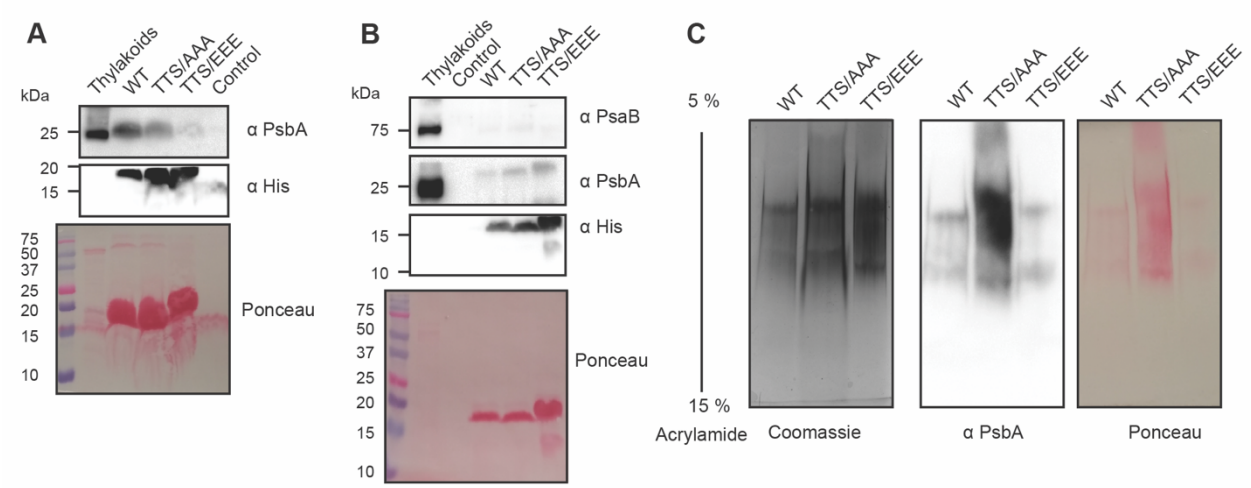

Figure 6. The phosphorylation status of ApcG influences its interaction with PSII. Pull-down experiments using the truncated form of ApcG with a mutated version for a permanent non-phosphorylated (TTS/AAA) and a phospho-mimicking version (TTS/EEE). Solubilized thylakoid membranes from the ApcG deletion strain were used to perform pull-down experiments. A representative experiment (one of four) is shown. **(A)** Western blot analysis for the detection of PSII marker protein PsbA pulled down by each ApcG version used. Anti-His antibodies were used to detect the three ApcG His-tagged versions. The experiment was performed using the same amount of truncated ApcG versions and solubilized thylakoids. **(B)** Pull-down experiment using three times more of the phospho-mimicking version (TTS/EEE) compared to wild type and permanent non-phosphorylated (TTS/AAA). Antibodies against marker proteins for PSII (PsbA) and PSI (PsaB) were used to detect the super-complexes pulled down by each truncated form of ApcG. **(C)** Native gel analysis for the pull down of PSII super-complexes (2 µg of protein loaded per lane). A Coomassie stained gel is shown as well as the immunoblot detection of PSII marker protein PsbA. Images from section **(A)** to **(C)** show a representative experiment from three biological replicates.

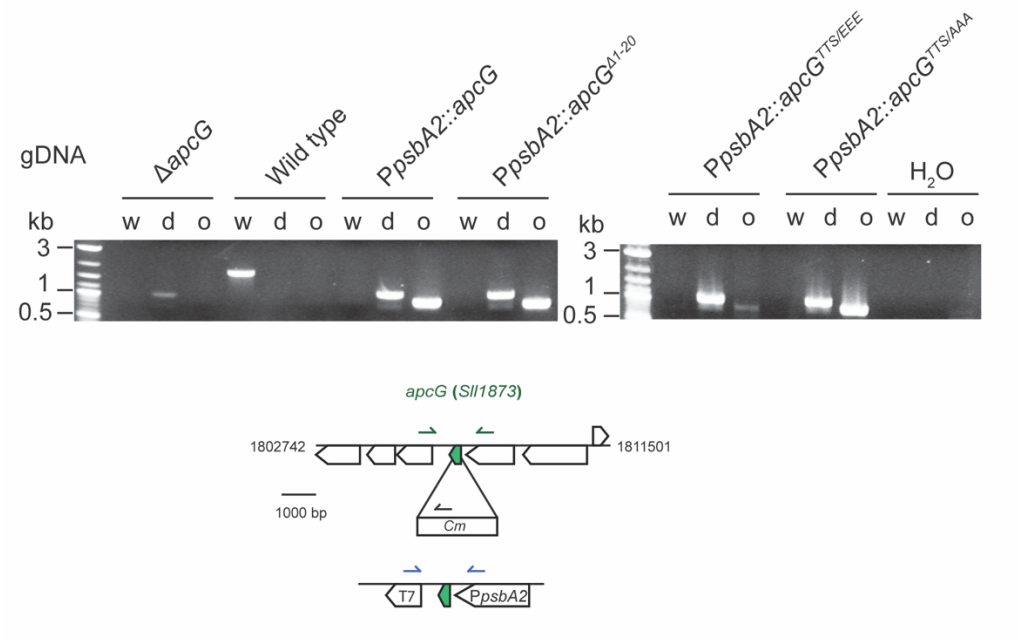

Supplemental figure S1. Genotyping of deletion and complementation strains of *apcG*. Genomic DNA (gDNA) was extracted from wild type, deletion, and the complementation strains to perform PCRs for the detection of the wild type allele (w), deletion cassette (d) or over-expression gene (o). In the lower panel it is shown the locus of *apcG* (*Sll1873*) as well as the primers used for each PCR reaction.

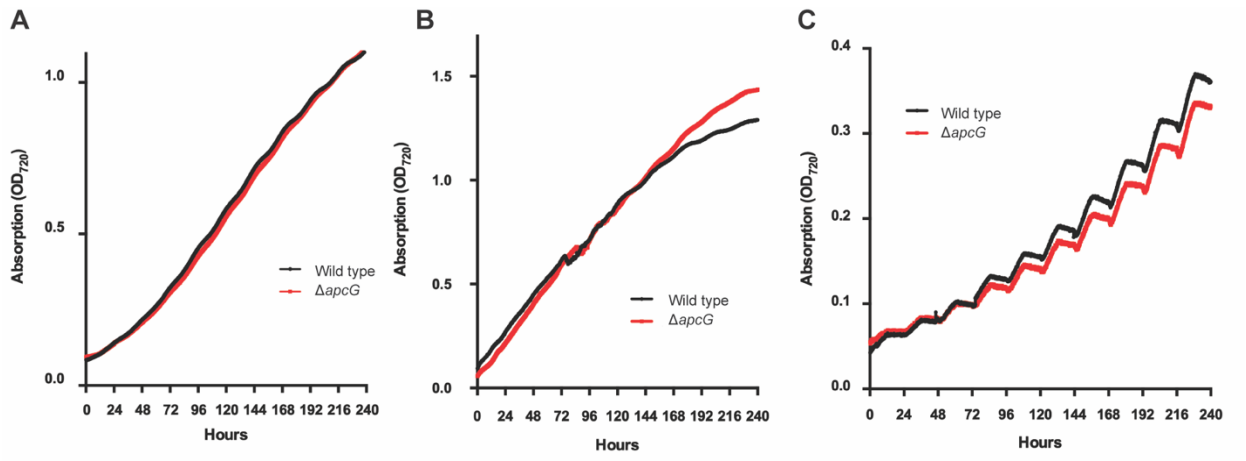

Supplemental figure S2. Growth curve comparison of the wild type and *apcG* deletion strains under normal and light stress conditions. Wild type and *apcG* deletion strains growth were compared under constant low light of 30 µmol photons $s^{-1} \cdot m^{-2}$ light intensity (**A**), constant high light of 400 µmol photons $s^{-1} \cdot m^{-2}$ light intensity **(B)** and light to dark periods of 12 hours each with 30 µmol photons $s^{-1} \cdot m^{-2}$ light intensity for the light periods **(C)**. Values correspond technical duplicates of a representative experiment from three biologically independent replicates. Growth curves were obtained with the instrument Multi-cultivator from PSI (MC 1000-OD) starting the cultures with 0.05 OD at 750 nm.

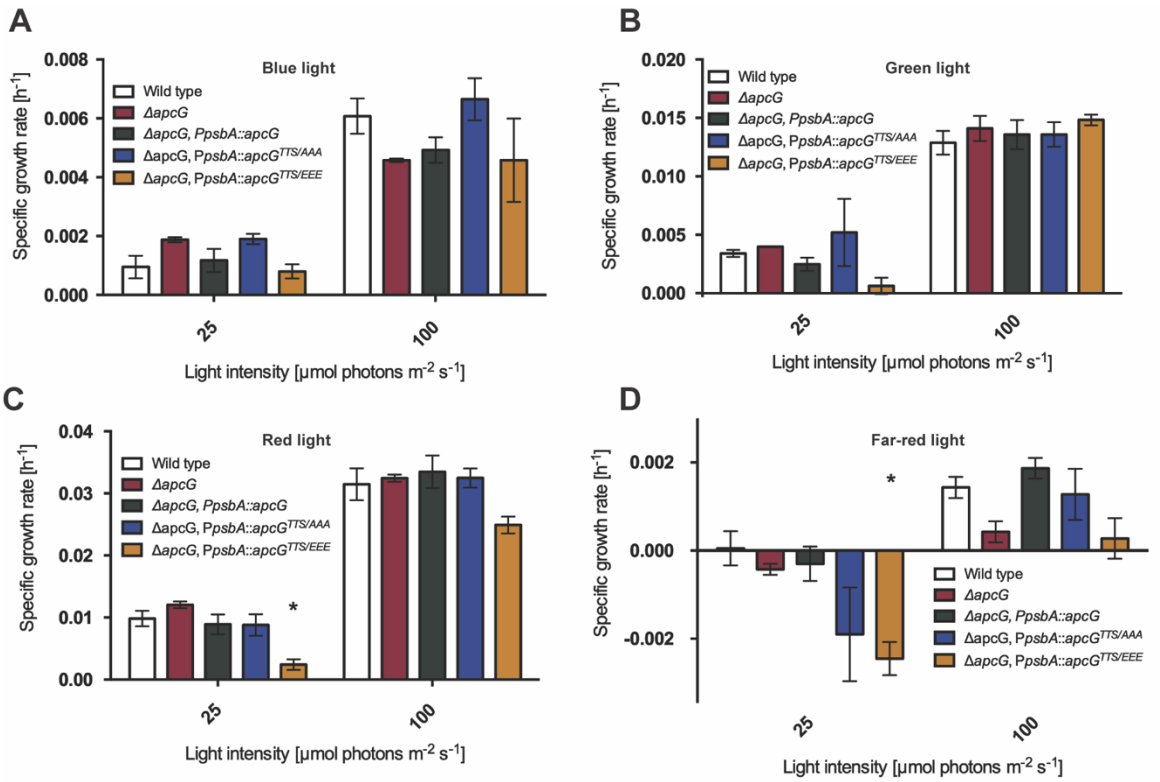

Supplemental figure S3. Comparison of growth in *apcG* strains under different light qualities and quantities. Cyanobacteria strains growth from *apcG* deletion, complementation strains and wild type was compared using blue light (**A**), green light (**B**), red light (**C**) and far-red light (**D**) under 25 and 100 µmol photons $m^{-2} \cdot s^{-1}$. Values represent means of four biological independent replicates and asterisks show statistical difference compared to wild type according to Student's *t* test (two-sided, $P < 0.05$)**.**

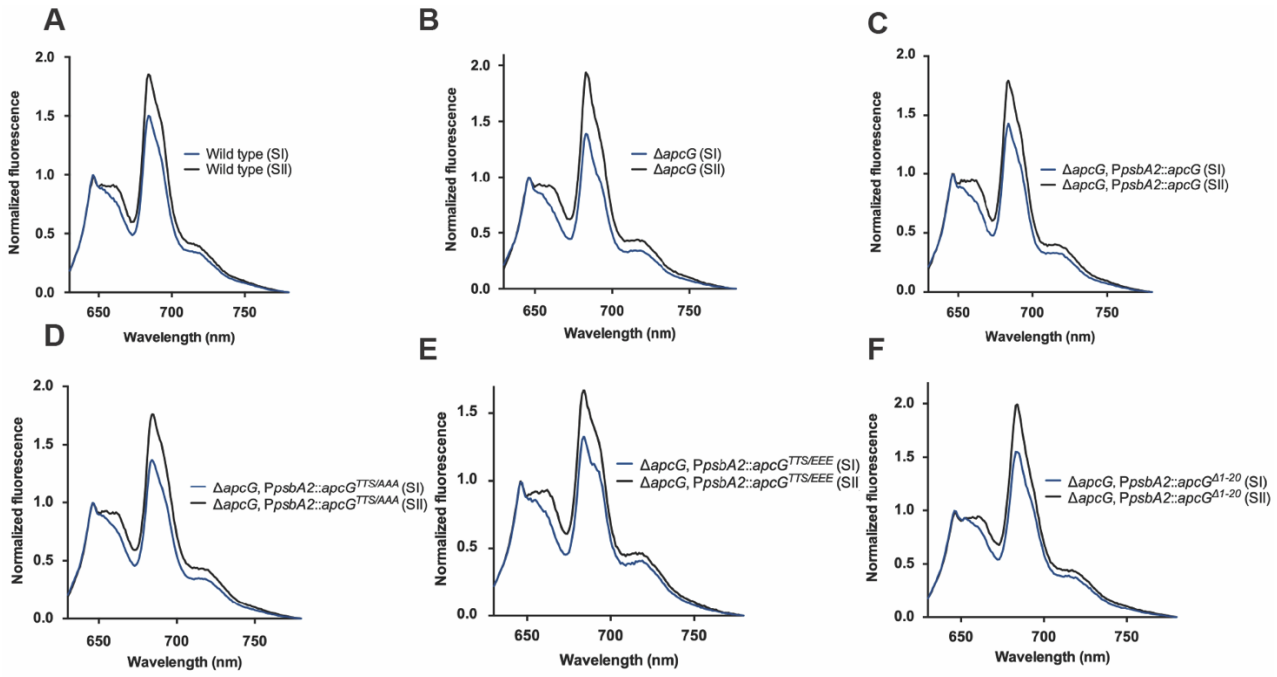

Supplemental figure S4. ApcG does not play a role in state transitions. Low temperature (77 K) fluorescence spectra from *Synechocystis* cultures were obtained under state I (induced with blue light pre-treatment) and state II (pre-treated under darkness). The strains used correspond to *Synechocystis* wild type (**A**), *apcG* deletion (**B**), *apcG* wild type complementation (**C**), permanent non-phosphorylated $apcG^{TTS/AAA}$ (**D**), phospho-mimicking $apcG^{TTS/EEE}$ (**E**) and truncated $apcG^{\Delta 1\text{-}20}$ (**F**). Values correspond to the mean of three biological replicates. Spectra were normalized to the peak of PBS at 646 nm.

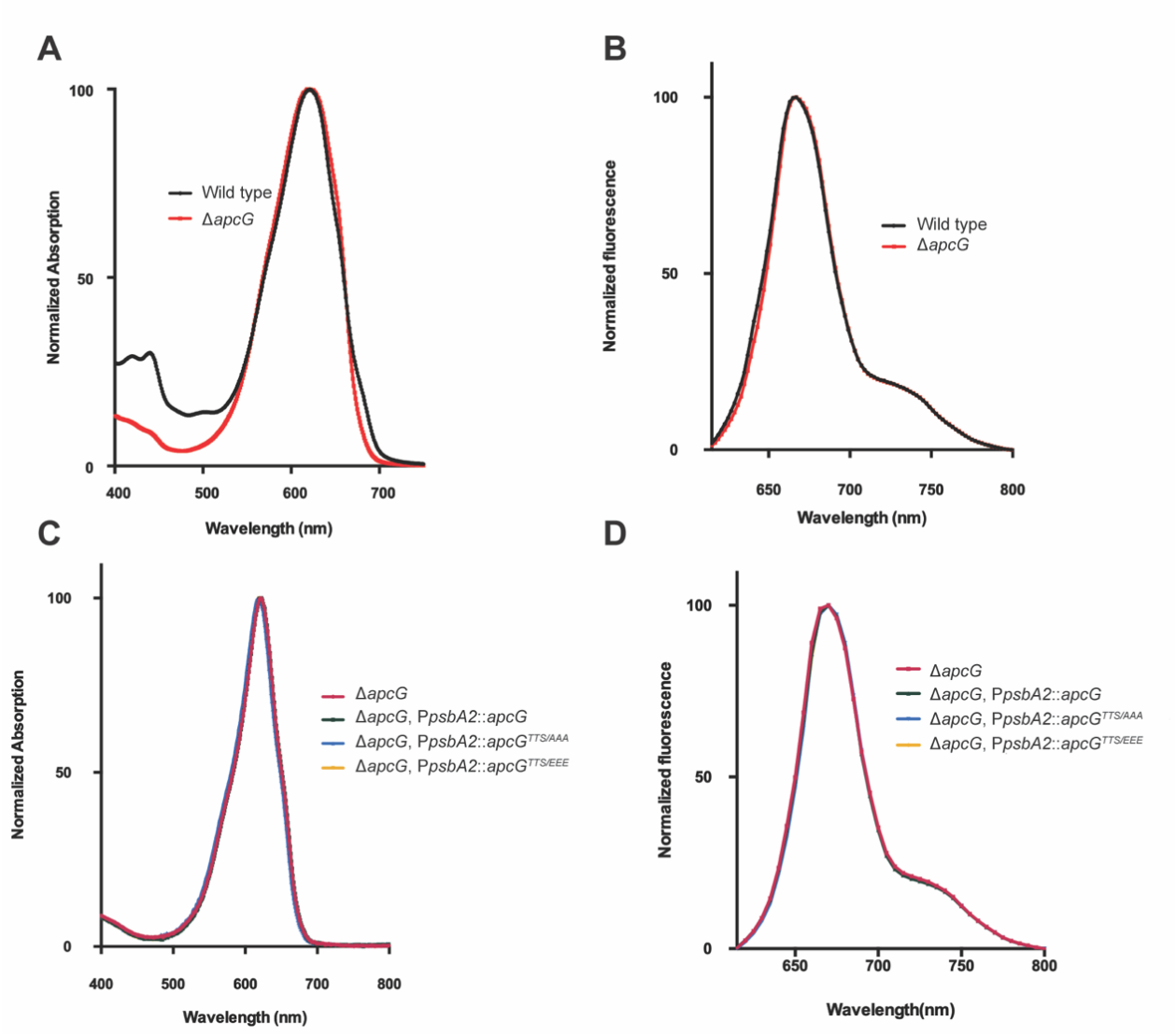

Supplemental figure S5. Absorption and fluorescence spectra of isolated PBS from deletion and complementation strains. PBS isolated after sucrose gradient were used to record their absorption and fluorescence spectra to assess their integrity. The wild type and *apcG* deletion strains absorption and fluorescence spectra are shown in **(A)** and **(B)** respectively. Additionally, comparison of PBS obtained from the deletion and complementation strains are shown in their respective absorption **(C)** and fluorescence **(D)** spectra. Values correspond to technical triplicates (normalized to their maxima) from a representative experiment out of three biologically independent samples.

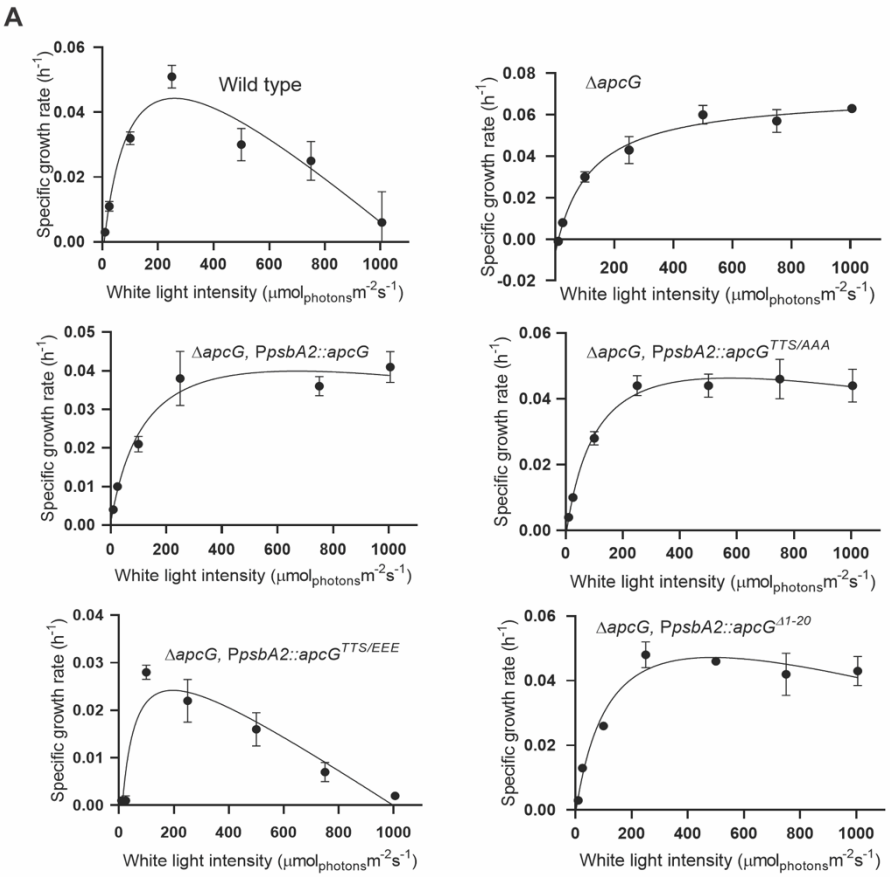
A
Wild type
ΔapcG
ΔapcG, PpsbA2::apcG
ΔapcG, PpsbA2::apcG^TTS/AAA
ΔapcG, PpsbA2::apcG^TTS/EEE
ΔapcG, PpsbA2::apcG^Δ1-20
Specific growth rate (h-1)
White light intensity (μmolphotons m-2 s-1)

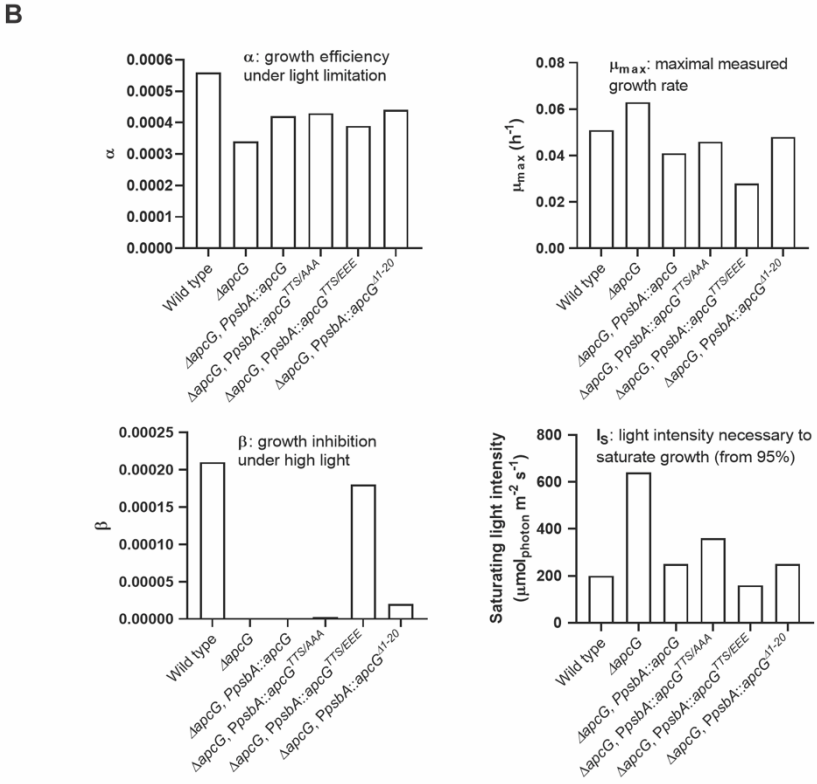
B
α: growth efficiency under light limitation
μmax: maximal measured growth rate
β: growth inhibition under high light
Is: light intensity necessary to saturate growth (from 95%)
Saturating light intensity (μmolphoton m-2 s-1)
Wild type
ΔapcG
ΔapcG, PpsbA::apcG
ΔapcG, PpsbA::apcG^TTS/AAA
ΔapcG, PpsbA::apcG^TTS/EEE
ΔapcG, PpsbA::apcG^Δ1-20

Supplemental figure S6. Growth curves of *apcG* strains under different high light intensities. Wild type, deletion, and complementation strains of *apcG* were grown under different white light intensities. (**A**) Specific growth curves for all strains under increasing light intensities starting from 10 to 1100 $\mu mol_{photon}\ m^{-2}\ s^{-1}$. Values correspond to mean of four biological replicates and error bars correspond to SEM. (**B**) Growth parameters of growth efficiency under light limitation (α), maximal measured growth (μ_{max}), growth inhibition under high light (β) and light intensity necessary to saturate growth (I_S). Values were calculated as described by Platt et al., (1980) for each curve from section **A**.

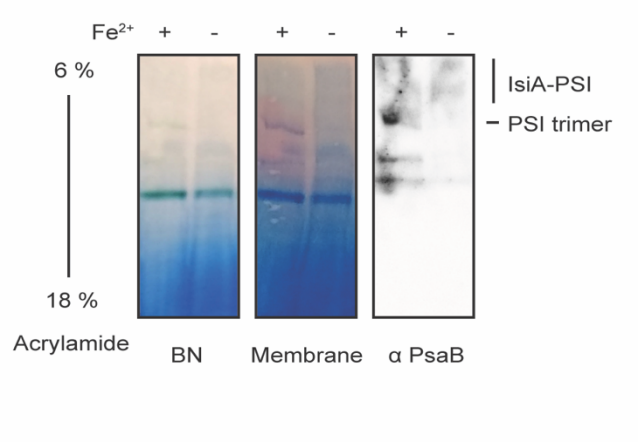

Supplemental figure S7. Absence of IsiA-PSI super complexes under normal growth conditions. Wild type *Synechocystis* strain was grown in normal BG-11 medium and one lacking iron for two days. Thylakoids membranes were extracted and solubilized to separate native super-complexes in a blue native gel. Afterwards, the proteins were transferred to a membrane and incubated with antibodies against PsaB (marker protein for PSI). Two micrograms of chlorophyll were loaded onto each lane. The position of PSI trimer and IsiA-PSI super-complexes are indicated as described by Duhring et al., (2006).

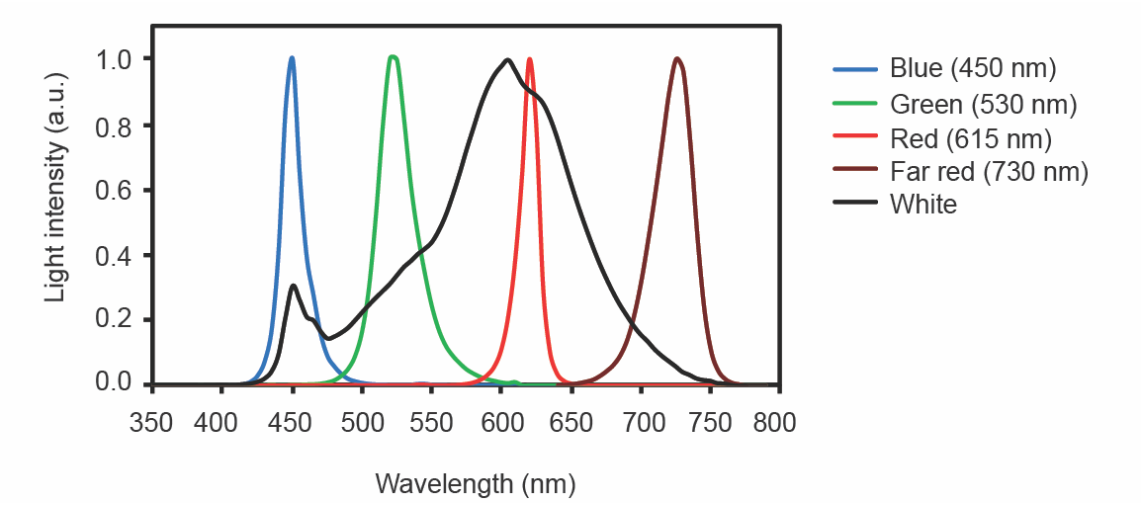

Supplemental figure S8. Light sources spectra. The light sources spectra used for growing cyanobacteria strains were recorded from 350 to 800 nm. Light intensity is represented as arbitrary units (a.u.) normalized to each color maxima.